Revision 3.

Thermodynamic properties of a saponite, a nontronite and a vermiculite derived from calorimetric measurements

Hélène Gailhanou[1,*], Philippe Blanc[1], Jacques Rogez[2], Georges Mikaelian[2], Katsuya Horiuchi[3], Yasuhisa Yamamura[3], Kazuya Saito[3], Hitoshi Kawaji[4], Fabienne Warmont[5], Jean-Marc Grenèche[6], Philippe Vieillard[7], Claire I. Fialips[8], Eric Giffaut[8] and Eric C. Gaucher[1]

[1]BRGM, 3 Av. C. Guillemin, BP6009, F-45060 Orleans, France

[2]IM2NP-CNRS Aix Marseille Université, FST Saint-Jérôme, F-13397 Marseille Cedex 20, France

[3]Department of Chemistry, Faculty of Pure and Applied Sciences, University of Tsukuba, Tsukuba, Ibaraki, 305-8571 Japan

[4]Tokyo Institute of Technology, 4259 Nagatsuta-cho, Midori-ku, Yokohama, 226-8503 Japan

[5]CRMD-CNRS, 1b Rue de la Ferollerie, F-45071 Orleans, France

[6]LUNAM, Université du Maine, Institut des Molécules et Matériaux du Mans, UMR CNRS 6283, F-72085 Le Mans Cedex 9, France

[7]CNRS-IC2MP-UMR-7285 Hydrasa, 5 Ave Albert Turpain, 86022 POITIERS-Cedex, France

[8]Andra, F-92298 Châtenay-Malabry Cedex, France.

Corresponding author:

Hélène GAILHANOU

BRGM, 3 Av. Claude Guillemin BP6009

45060 Orleans, France.

* Email: h.gailhanou@brgm.fr

Abstract --- The stability of clay minerals is an important factor in assessing the durability of containment barriers for deep waste storage. In that context, the complete thermodynamic dataset of three 2:1 ferro-magnesian clay minerals have been determined at 1 bar and from 2 K to 520 K, using calorimetric methods. The studied clay samples were respectively, the Na-saturated saponite Sap-Ca-1, $Na_{0.394}K_{0.021}Ca_{0.038}(Si_{3.569}Al_{0.397}Fe^{3+}_{0.034})(Mg_{2.948}Fe^{2+}_{0.021}Mn_{0.001})O_{10}(OH)_2$, the Ca-saturated nontronite NAu-1, $Ca_{0.247}K_{0.020}(Si_{3.458}Al_{0.542})(Mg_{0.066}Fe^{3+}_{1.688}Al_{0.268}Ti_{0.007})O_{10}(OH)_2$, and the Ca-saturated Santa Olalla vermiculite, $Ca_{0.445}(Si_{2.778}Al_{1.222})(Al_{0.192}Mg_{2.468}Fe^{3+}_{0.226}Fe^{2+}_{0.028}Ti_{0.018}Mn_{0.007})O_{10}(OH)_2$. The standard enthalpies of formation were obtained by solution-reaction calorimetry at 298.15 K. The heat capacities were measured between 2 K and 520 K, using low-temperature adiabatic calorimetry, heat-pulse calorimetry and differential scanning calorimetry. The standard entropies and the Gibbs free energies of formation at 298.15 K have been calculated from these values. Finally, the equilibrium constants at 298.15 K have been determined and the following thermodynamic properties have been retrieved at 298.15 K and 1 bar:

	ΔH_f^0 kJ/mol	C_p^0 J/(K·mol)	S^0 J/(K·mol)	ΔG_f^0 kJ/mol
Saponite, dehydrated	-5993.84 (± 4.86)	347.20 (± 1.74)	314.59 (± 1.56)	-5622.24 (± 4.88)
Nontronite, dehydrated	-5034.39 (± 5.33)	335.16 (± 0.33)	332.85 (± 7.04)	-4683.56 (± 5.73)
Nontronite, n = 5.978 H_2O a.p.f.u.	-6774.32 (± 5.61)	n.d.	n.d.	n.d.
Vermiculite, dehydrated	-6030.34 (± 5.70)	346.70 (± 0.35)	326.08 (± 0.48)	-5662.23 (± 5.71)

Note. a.p.f.u. atom per formula unit, on the basis of an $O_{10}(OH)_2$ unit
n.d.: not determined

A comparison between these experimental data and estimated values obtained from prediction models available in the literature enabled the most usual calculation methods available to date to be assessed for each thermodynamic property.

Keywords: clay mineral, saponite, nontronite, vermiculite, thermodynamic data, enthalpy, Gibbs free energy, entropy, calorimetry, dissolution.

INTRODUCTION

The thermodynamic properties of clay minerals are intrinsic properties, essential for the prediction of the chemical behaviour of clayrocks, soils or artificial materials (engineered barriers, additives, etc.). For deep disposal applications especially, such as radioactive wastes storage within clay rock formations, clay minerals represent an essential component of the engineered barrier system or of the surrounding clayrock, which acts as the final component of the barrier system. In order to assess the stability of barrier concepts over long time periods (typically more than 1000 centuries), geochemical modelling is a valuable tool for predicting mineralogical and chemical evolution (Gaucher and Blanc 2006). Thermodynamic properties are essential for such applications. An example of such data is given in a recent paper (Gailhanou et al., 2012) reporting the results obtained by direct measurements of the thermodynamic properties of 2:1 aluminous clay minerals (smectite, illite and beidellite).

The present work focuses on measuring the thermodynamic properties of ferro-magnesian 2:1 clay minerals, nontronite, saponite and vermiculite, since consistent datasets are not as yet available for such minerals. Within the context of deep disposal applications, Gailhanou et al. (2012) have mainly focused their studies on minerals that could be initially present in the barrier system. Now, the present work concerns the measurement of the thermodynamic functions of minerals that could be produced during possible transformations of the clay barrier. Indeed, in previous experimental studies (Nagy et al. 2000; Cuevas 2005), saponite has been characterised among the final products after experimental alteration of aluminous smectite by an alkaline solution. Similarly, the formation of saponite is predicted by geochemical calculations (Savage et al. 2002; Gaucher et al. 2004), resulting from the long-term interaction between an aluminous-smectite based engineered barrier and a cement plug. Additionally, a large amount of experimental works have been conducted concerning

iron/clay interactions. These studies (Guillaume et al. 2004; Charpentier et al. 2006; Lantenois et al. 2005; Wilson et al. 2006) account for the presence of an iron canister among the engineered barrier system and the possible mineralogical modifications of clay minerals in contact with iron enriched solutions. The review by Mosser-Ruck et al. (2010) shows that rather distinct mineral changes and sequences can be distinguished, depending on physical-chemical parameters such as temperature, pH, iron/clay and liquid/clay ratios. Between 80 and 150°C, smectite may either be enriched in iron and then form a nontronic component, or it may be completely transformed into 7 Å clay minerals (e.g. berthierine, cronstedtite). For temperatures higher than 150 °C, it may be transformed into Fe-rich saponite and then into trioctahedral chlorite or into Fe-rich vermiculite.

In light of these previous works, the need for accurate and directly measured thermodynamic properties is clearly apparent in order to limit the uncertainties in the long-term geochemical calculations where these phases precipitate. To our knowledge, only Kalinowski and Schweda (2007) have measured the equilibrium constant for a vermiculite mineral and no experiments or measurements have been performed on saponite or nontronite minerals to date. The present study aims to make up for the lack of reliable data concerning these minerals.

The method adopted for this study is similar to that described in Gailhanou et al. (2012) for illite, smectite and beidellite and was adapted from the method of Johnson et al. (1992) on mordenite. The present study combines, for each phase, different calorimetric methods:

- Low temperature acidic solution calorimetry for ΔH_f^0.
- Low temperature adiabatic calorimetry for S^0.
- Differential scanning calorimetry (DSC) for $C_p{}^0(T)$ ($T > 25$ °C).

In the present work, the mineralogical characterization of the samples is first detailed and the calorimetric methods are then described from a general viewpoint. The results of the

measurements are reported in a second part. For each sample, the present data are finally compared with the results of the available estimation methods.

MATERIALS AND METHODS

Clay Samples

The studied saponite and nontronite samples came from the Source Clay Project of the Clay Minerals Society. These are saponite Sap-Ca-1 from Ballarat (California, USA; Post 1984) and nontronite NAu-1 from the Uley graphite mine (South Australia; Keeling et al. 2000). The vermiculite sample came from Santa Olalla (Huelva Spain; Norrish 1973; Pérez-Maqueda et al. 2001).

Sample preparation. The < 2 μm size-fraction of the saponite sample was first separated by centrifugation. Then, it was treated with 0.1 M acetic acid in 0.5 M NaCl solution to remove carbonates. After washing with 0.5 M NaCl, the solid was treated for the removal of iron oxide and (oxy)hydroxides using a citrate-bicarbonate-dithionite method (CBD) adapted from the Mehra and Jackson (1958) procedure. The solid was suspended in a 0.2 M sodium citrate solution, and a NaOH solution was added to adjust the pH to 6. The suspension was heated to 40 °C and sodium dithionite was added until the redox potential was adjusted to about 0 V. After centrifugation, the solid was treated with H_2O_2 (3%) at 60 °C to remove the organic matter. The saponite sample was then centrifuged and Na-saturated using 1 M NaCl solution. After washing in a 10^{-2} M NaCl solution, the concentration of chloride ions at 10^{-2} M was checked by ion chromatography. The 10^{-2} M NaCl solution was preferred to deionized water in order to avoid the swelling of the clay generating some gel, which is too difficult to be washed correctly. The solid was centrifuged before drying at 40°C for several days. The absence of halite in the solid was checked by X-ray diffraction (XRD).

In the same way as for the saponite sample, the < 2 μm size-fraction of the nontronite sample was first separated by centrifugation. Then, the nontronite sample was Ca-saturated in a 1 M $CaCl_2$ solution for 24 h. After washing the solid in deionized water, the absence of chloride ions was checked using the $AgNO_3$ test.

The vermiculite sample was first treated using the CBD treatment to remove aluminium hydroxides. After centrifugation, organic matter was removed by using the previous treatment with H_2O_2. The solid was then Ca-saturated in a 1 M $CaCl_2$ solution and then washed in deionized water. The absence of chloride ions in the suspension was checked using the $AgNO_3$ test.

Finally, the three treated samples were dried at 40 °C for several days and hand ground in an agate mortar. They were then maintained at ambient pressure, temperature and relative humidity (1 bar, 25 °C, close to 75% RH) during the characterization process. In the following, 'samples' or 'samples at ambient humidity' will mean 'after the preceding treatments'. They correspond to the purified clay minerals, including some remaining impurities.

Analysis and characterization of the samples. Chemical analyses for Si, Al, Ti, Fe (total), Mn, Ca, Mg, K, Na and P were performed by X-ray fluorescence spectroscopy. The amounts of inorganic carbon, total carbon and total sulphur were obtained using volumetric methods detailed in Gailhanou et al. (2007, 2009). The results of chemical analyses are presented in Table 1, in wt% of oxides.

XRD analyses were performed on a Siemens D5000 diffractometer equipped with variable slits, a Co anticathode and a diffracted beam monochromator to characterize and quantify impurities and clay phases. To determine the abundances of clay and non-clay minerals, a powder X-ray diffractogram was first acquired, on each sample, from 4 to 84 °2θ with a rotation speed of 0.002 °2θ/s. Powder samples were top-loaded into the 2.5 cm diameter

sample holder cavity without compaction to preserve random orientation (Hillier, 2000). The proportions of impurities were obtained by applying a least-squares fit method using XRD patterns of individual phases calculated with PowderCell 2.3 (Kraus and Nolze 2000). To analyse the clay phases in more detail, X-ray diffractograms were also acquired on oriented deposits on a glass slide, from 2 to 36 °2θ with a rotation speed of 0.01 °2θ/s. The clay phases were quantified using the model of Blanc et al. (2007), which is based on a linear combination of patterns of clay minerals, simulated with NEWMOD (Reynolds 1985).

The proportions of ferric and ferrous ions in the clay minerals and, if present, the amounts of ferrous or ferric impurities were determined by ^{57}Fe Mössbauer spectrometry. These analyses were performed using a conventional constant acceleration Mössbauer spectrometer, in transmission geometry, equipped with a ^{57}Co(Rh) source. The isomer shift values were corrected according to the calibration of the velocity scale made from α-Fe at 300 K. For each spectrum, the amount of Fe in the sample was about 5 mg/cm^2.

The compositional homogeneity of the minerals with regard to the major elements Si, Al, Fe, Mg, Na, Ca, K, Ti and Mn was checked by microprobe analyses, performed using a CAMEBAX SX50 - 15 kV accelerating voltage, 12 nA beam-current intensity and 1–2 μm beam width. The counting time was 10 s for major elements Si, Al, Fe, Mg, Na, Ca, K, Mn and Ti. Standards used included both well-characterized natural minerals and synthetic oxides. Matrix corrections were performed using the PAP procedure (Pouchou and Pichouar, 1984). The chemical analyses are expressed in wt% oxides. The Principal Components Analysis (PCA) method (XLSTAT©, 2006) was used to perform the statistical treatment of microprobe analyses. This multivariate method makes it possible to detect and to identify graphically the potential dispersions of the chemical compositions. Moreover, it also aims to elucidate the links between the chemical elements in the structure, on the basis of the representation of the multiple correlations.

In the saponite sample, the amounts of mineral impurities detected by XRD were estimated (in wt%) at 1.25% amphibole, 1% diopside, 0.3% muscovite and 0.25% quartz. The nature of the amphibole, determined by microprobe analyses, was a tremolite. Moreover, some analyses exhibited a very high Ti content, suggesting the presence of TiO_2 impurities. Some complementary transmission electron microscopy (TEM) observations confirmed the presence of a few clusters of TiO_2 impurities. Furthermore, after removing diopside, tremolite and Ti rich compositions, 184 microprobe analyses were treated using the PCA method. It resulted that the first main eigenvectors $\mathbf{F_1}$ and $\mathbf{F_2}$ account for a moderate part (49%) of variance (Fig. 1). Ca has a high and negative loading to $\mathbf{F_1}$, suggesting that the variability of compositions was partly explained by the presence of some Ca-rich compositions, corresponding probably to analyses of assemblages of saponite and diopside or tremolite impurities. Nevertheless, the variability of chemical compositions was rather low, as shown by the low standard deviations on the Si, Al and Mg compositions, respectively at 1%, 6% and 3%. These results suggest a good chemical homogeneity of saponite particles.

Furthermore, from the modelling of ^{57}Fe Mössbauer spectra at 77 K and 300 K performed on the saponite sample, the proportions of ferrous and ferric ions have been estimated at 44 at% Fe^{2+} ($\pm$ 2 at%) and 56 at.% Fe^{3+} ($\pm$ 2 at%), respectively. Moreover, ferric ions are exclusively located in tetrahedral sites, whereas ferrous ions are distributed in two octahedral sites. Furthermore, for the saponite sample, a ^{27}Al NMR spectrum was realized using a Bruker DSX400 with a 12 kHz rotation speed. The spectrum exhibited a main magnetic resonance at 64.7 ppm, associated with tetrahedral aluminium (~ 98.5% of total Al), and a small resonance at 2.9 ppm, corresponding to octahedral aluminium (~ 1.5% of total Al).

For the nontronite sample, XRD analyses revealed the presence of kaolinite (6.2 wt%), goethite (2 wt%) and quartz (0.2 wt%). Furthermore, the modelling of ^{57}Fe Mössbauer spectra performed at 77 K and 300 K results from two main components: the quadrupolar feature

described by two quadrupolar doublets associated with *a priori* ferric ion species in an octahedral environment of nontronite, and the magnetic component consisting of at least two magnetic sextets clearly attributed to ferric ions in goethite (Fig. 2). In addition, no high spin ferrous ions were detected in nontronite. It should be mentioned that a low spin ferrous component such as pyrite is excluded because no S occurs in the elemental composition, thus allowing the quadrupolar component to be unambiguously attributed to ferric species. The refined values of corresponding Mössbauer hyperfine parameters are listed in Table 2. The amount of goethite was estimated at 2 wt%, in very good agreement with the XRD results. Finally, 181 microprobe analyses were statistically treated using the PCA method to assess the chemical homogeneity of nontronite. The first main eigenvectors $\mathbf{F_1}$ and $\mathbf{F_2}$ account for a low percentage (38%) of variance, which is significant of a good chemical homogeneity of the sample (Fig.1). The standard deviations on the Si, Al and Fe compositions are low, respectively 1%, 4% and 4%. Consequently, nontronite particles have a high chemical homogeneity.

Concerning the vermiculite sample, XRD analyses revealed the presence of 0.5%wt quartz and 0.15%wt cristobalite (Table 3). Modelling of the ^{57}Fe Mössbauer spectra at 77 K and 300 K leads to an estimate of the proportions of ferrous and ferric ions, respectively at 11 at.% of total Fe for Fe^{2+} and 89 at.% for Fe^{3+}. Moreover, some microprobe analyses were performed on 194 compositions and treated using the PCA method. The main eigenvectors $\mathbf{F_1}$ and $\mathbf{F_2}$ account for 37% of variance and $\mathbf{F_1}$ and $\mathbf{F_3}$ for 32% of variance. These low values reveal that there is only one population of vermiculite particles, with similar compositions. More precisely, the strong anti-correlation between silica and magnesium (91%) is well described by $\mathbf{F_1}$ and $\mathbf{F_2}$. $\mathbf{F_1}$ also shows a weaker anti-correlation between aluminium and magnesium (40%) (Fig. 1). Silica and aluminium elements are weakly correlated (7%). From these results, the following substitutions may be expressed in tetrahedral and octahedral sites:

224 $Si^{IV} + Al^{VI} = 2\ Mg + Al^{IV}$

225 Finally, the amounts of impurities in the three clay samples, determined at ambient RH, are
226 given in Table 3. The impurity contents in the dehydrated state were also calculated from the
227 values discussed previously, by removing the water mass expelled after 20h at 150°C from
228 the compositions of the samples initially maintained at ambient RH (Table 3).
229 The structural formulae of the clay minerals (Table 4) are calculated from the overall
230 chemical compositions (Table 1), corrected by removal of the contributions of impurities
231 determined at ambient RH (Table 3).
232 For vermiculite, the average structural formula obtained from microprobe analyses,
233 $Ca_{0.47}Na_{0.02}Si_{2.76}Al_{1.43}Mg_{2.43}Fe_{0.26}Ti_{0.02}Mn_{0.01}O_{10}(OH)_2$, is in very good agreement with the
234 previous result. Such a comparison was limited to the vermiculite sample, since for the
235 nontronite and saponite samples some of the microprobe compositions corresponded to
236 mixtures of clay and impurities.
237 The structural formula of saponite is in very good agreement with those given by Toranzo et
238 al. (1998) and Bergaoui et al. (1995), despite the fact that these do not contain ferric ion in
239 tetrahedral layers. These formulae differ from that provided by Post (1984), which contains
240 more Si, i.e., 0.2 Si atom per formula unit (a.p.f.u.). For nontronite NAu-1, the formula is
241 rather close to that provided by Keeling et al. (2000), with only a difference expressed by the
242 substitution of 0.15 Fe^{3+} by 0.15 Al a.p.f.u. in the present formula. The structural formula of
243 Santa Olalla vermiculite is consistent with those available in the literature (Norrish 1973; de
244 la Calle 1977; Suquet and Pezerat 1987; Pérez-Maqueda et al. 2001; Argüelles et al. 2010).
245 **Molar volumes.** Following Gailhanou et al. (2012), the values of unit-cell parameters
246 *a*, *b* and *c* were determined from powder and oriented XRD diffractograms and from the (001)
247 and (060) peak positions of each sample, considering a monoclinic space group for each
248 sample, and the approximation $a = \frac{b}{\sqrt{3}}$ proposed by Drits and Tchoubar (1990). The β angle

was chosen at 96.1° for saponite (Gournis et al. 2008), 101° for nontronite (Manceau et al. 1998) and 95.16° for vermiculite (Shirozu and Bailey 1966). The calculated molar volumes, for both hydration states, are reported in Table 5, from XRD measurements performed on air-dried samples (ambient RH) and samples heated to 490 °C for 2 hours (dehydrated). Calculation details are reported in Gailhanou et al. (2012).

Hydration states of samples for calorimetric measurements. The present work aims to establish the thermodynamic functions of clay minerals mainly in dehydrated states. Dehydrated states of saponite and nontronite samples were obtained after heating the samples to 150 °C for 20 hours (Gailhanou et al. 2007, 2012). For vermiculite, thermogravimetric analyses of Mg-vermiculite from Santa Olalla by Argüelles et al. (2010), revealed two dehydration stages of interlayer cations, respectively at 120 °C and 240 °C. According to these authors, the former could correspond to the loss of the second water layer in the interlayer space, whereas the latter could be associated with the loss of the first water layer. In the present study concerning Ca-vermiculite, thermogravimetric analyses were carried out by heating the samples from 25 °C to 400 °C, at a controlled heating rate (2 °C/min) (Fig. 3). The derivative of the mass loss curve versus temperature (DTG curve in Fig. 3) shows two peaks at 90 and 185 °C corresponding to the two dehydration stages described by Argüelles et al. (2010), respectively. According to these results, the vermiculite sample was dehydrated at 215 °C for 20 hours.

The hydrated state of the nontronite sample was obtained by monitoring the relative humidity (RH) at 75% with oversaturated sodium chloride solution at 22.2 °C. Equilibrium attainment was followed by checking the sample mass. The adsorbed amount of water was determined by weighing the samples after dehydration at 150 °C for 20 hours.

Calorimetric methods

Heat capacity measurements. The heat capacities were measured on dehydrated samples between 8 K and 520 K for the saponite sample and from 2 K to 520 K for the nontronite and the vermiculite samples, using several techniques. These measurements aimed to determine the $C_p^0(T)$ functions and the entropies at 298 K of the clay minerals in dehydrated states.

For saponite Sap-Ca-1, heat capacities were measured in the temperature range 8 K – 377 K using a low-temperature adiabatic calorimeter (low-TAC) described by Yamamura et al. (1995). The dehydrated sample, weighing 2.9837 g (± 0.0002 g) after the buoyancy correction was sealed under a dry helium atmosphere in a gold-plated copper calorimeter vessel with helium gas (10^5 Pa) at room temperature. A platinum (Minco, S1055) resistance thermometer was used for thermometry based on the ITS-90. The accuracy of the measurements, assessed using a standard reference material (SRM 720, synthetic sapphire, U.S. National Bureau of Standards), was better than 0.5% above 50 K. Maximum deviations of 0.1% were recorded at temperatures above 50 K.

For the nontronite and vermiculite samples, the heat capacities were measured by heat pulse calorimetry between 2 K and 50 K, using a commercial apparatus (PPMS model 6000, Quantum Design Inc.; Dachs and Bertoldi 2005). Measurements were performed twice in the temperature range by cooling and by heating the samples, respectively. The amounts of sample were 12.01 mg and 4.19 mg for the nontronite and vermiculite samples, respectively. Moreover, the measurements were performed by low-TAC between 14 K and 310 K for the nontronite sample and between 14 K and 327 K for the vermiculite sample, using an adiabatic calorimeter described by Atake et al. (1990). In both cases, the dehydrated sample was first loaded in a calorimeter vessel, in a glove box under dry nitrogen atmosphere. It was then evacuated using an oil diffusion pump with a liquid nitrogen trap at room temperature for 24

hours. Afterwards, a small amount of He gas (10 kPa for the nontronite sample and 38 kPa for the vermiculite sample) was introduced into the vessel for improving the heat exchanges, and the vessel was then tightly sealed. The amounts of clay samples were respectively 10.5979 g and 7.1775 g for the nontronite and the vermiculite samples. The maximum deviations expected in the measurements of the Cp of the clays, calibrated with measurements of synthetic sapphire (SRM 720, U.S. National Bureau of Standards), range from 5% at 15 K to 0.3% at 50 K and 0.1% above 100 K.

Finally, the heat capacities were measured by differential scanning calorimetry (DSC) in the temperature range 330 K – 520 K for the nontronite and the vermiculite samples and between 380 K and 520 K for the saponite sample. The calorimeter was a Calvet DSC111 differential scanning calorimeter from Setaram. The stainless steel vessel, with a volume of 0.18 cm^3, was filled with about 140 mg of a dehydrated clay sample and sealed with a nickel ring, under a nitrogen atmosphere. The DSC calibrations on the one hand for the temperature and enthalpy and for the heat capacity on the other hand consisted in commonly used procedures. Standard samples of indium (Goodfellow, purity 99.999%), zinc (Goodfellow, purity 99.999%) and aluminium (Goodfellow, purity 99.999%) were used for the temperature and the enthalpy calibration (Stølen and Grønvold 1999), and synthetic sapphire (U.S. National Bureau of Standards; Ditmars et al. 1982) for the heat capacity calibration. The calibration runs were performed under the same conditions of nitrogen flow rate and heating rate (2 K/min) as for the C_p^0 measurements on the clay samples. The intermittent method was implemented with 2.5 K steps for the measurement period, alternated with a temperature stabilization period of 600 s, in which the heat flow recovered the baseline value. At least two sets of runs were carried out for each material (blank, standard and sample runs).

Acid solution calorimetry at 298.15 K. Solution-reaction calorimetry was used to determine the standard enthalpies of formation at 298.15 K of the saponite and the vermiculite

322 samples in dehydrated states and of the nontronite sample in dehydrated and hydrated states.
323 The enthalpies of dissolution at 298.15 K were measured in a hydrofluoric and nitric acid
324 solution with a highly sensitive Tian-Calvet isothermal calorimeter, the Calsol calorimeter
325 (Ganteaume et al. 1991). The experimental procedure for these measurements on clay samples
326 has already been described by Gailhanou et al. (2012). The amount of sample was about 40
327 mg and the volume of acid solution was 50 mL. In particular, careful weighing of the samples
328 and filling of the calorimetric vessel made it possible to prevent hydration of the sample.
329 These operations were carried out in a glove box with dry argon for the dehydrated sample,
330 and in a room with controlled relative humidity and temperature (up to 80% max. at 22 °C)
331 for the hydrated sample. For this latter case, the adsorption or desorption of water during the
332 weighing was controlled and was found to be negligible.
333 The method used to determine the standard enthalpy of formation of the clay minerals at
334 298.15 K has been described in detail by Gailhanou et al. (2012). A first stage consists in
335 obtaining the enthalpy of formation of the clay mineral from the chosen secondary
336 thermodynamic references among oxides, hydroxides and nitrates, at 298.15 K. For this
337 purpose, the following enthalpies of reactions were measured for a given clay mineral: (i)
338 dissolution of the clay sample including the impurities, (ii) dissolution of a mixture of the
339 chosen secondary references of the clay mineral added to the impurities with the same
340 elemental quantities as those present in the sample, (iii) dilution type reactions.
341 The principle of this method based on the dissolution of the mixture of secondary references
342 and impurities and on the dissolution of the clay sample is to obtain the same final
343 equilibrium state after the dissolution reactions. In particular, at the end of the reactions, the
344 interactions between dissolved species themselves and dissolved species and solution are
345 expected to be identical. This is necessary for applying algebraic summation of the reactions
346 in order to obtain the reaction of formation of the clay mineral from the secondary references.

In the present study, the secondary references were selected among oxides, hydroxides and nitrates. The selection criteria were the purity of the compounds, their ability to be dissolved easily in the hydrofluoric and nitric acid solutions and the availability and reliability of the standard enthalpies of formation data in the literature (Appendix 1). Each selected compound is chemically non-reactive with the others at 25°C and with the air atmosphere especially with the ambient relative humidity, except for KOH, hygroscopic, and FeO, which can be oxidized under air atmosphere and form non-stoichiometric oxide. The use of KOH was restricted to the study of saponite, which contains a very low amount of potassium, and was handled very carefully during the preparation of the mixture to avoid its hydration. Moreover, the impact of the reactivity of FeO with air has been assessed on the final values of the enthalpies of formation of the studied clay minerals, and is negligible.

For each measurement on the mixture of the secondary references and impurities, the masses of the secondary references (except for H_2O) were weighed to provide the same elemental quantities than those present in the clay mineral for 40 mg of anhydrous clay sample. The impurities are added to the mixture of secondary references in the same amounts than those present in the clay sample.

Four or five measurements of solution enthalpies were performed for each type of reaction. Relative uncertainties for enthalpy measurements were lower than 0.5%.

The reaction of formation of a hydrated clay mineral at n H_2O per $O_{10}(OH)_2$ formula unit, from the secondary reference constituents is given by:

$$\sum_i n_i \; constituent_i * + m\,H_2O \rightarrow clay, n\,H_2O + n_{HNO_3}\,HNO_3 \qquad \text{(R. 1)}$$

where m is calculated from the balance on O and H associated with the structural hydroxyl groups, the adsorbed water quantity in clay and with the O and H contents of the secondary references, and n_{HNO3} is calculated from the balance on nitrates associated with HNO_3 and

with possible nitrates secondary references. The superscript (*) refers to all constituents except for H_2O.

Therefore, the enthalpy of formation per mole of clay mineral from the secondary reference constituents $\Delta H^0_{f/constit}$ at 298.15 K, may be expressed by (Gailhanou et al. 2012):

$$\Delta H^0_{f/constit} = \left(\frac{M_{\min}}{\eta} + (n-m)\,M_{H_2O} + n_{HNO_3} M_{HNO_3}\right)\Delta H_{diss,mixt} - \left(\frac{M_{\min}}{\eta} + n\,M_{H_2O}\right)\Delta H_{diss,sample} + m\,M_{H_2O}\,\Delta H_{dil} - n_{HNO3}\,M_{HNO_3}\Delta H_{sol} \quad (1)$$

where M_{min} is the molar mass of the dehydrated clay mineral, η is the mass fraction of the dehydrated clay in the dehydrated sample, n is the number of moles of water adsorbed by the clay, m and n_{HNO3} are respectively the numbers of moles of H_2O and HNO_3 expressed in mol/mol of clay. $\Delta H_{diss\ mixt}$, $\Delta H_{diss\ sample}$, ΔH_{dil} and ΔH_{sol} are respectively the enthalpy of dissolution of the mixture of the secondary references and the impurities, the enthalpy of dissolution of the clay sample, the enthalpy of dilution of the solvent and the integral enthalpy of mixing of pure HNO_3 in HF-HNO_3 solution.

Finally, in order to calculate the standard enthalpy of formation ΔH_f^0, a reference change is necessary using the standard enthalpies of formation of these secondary references provided by the literature (Appendix 1).

RESULTS

Heat capacities

Heat capacities of the samples. The heat capacity data measured for the three clay samples in the dehydrated states, using PPMS, low-temperature adiabatic calorimetry and DSC, are reported in Appendix 2. In the very low-temperature range, the values obtained by PPMS and low-TAC techniques are in good agreement, except for domains associated with C_p anomalies (Fig. 4). In the high temperature range, the slight systematic difference observed

between low-TAC and DSC measurements for the Sap-Ca-1 is probably due to a DSC calibration defect.

For both the saponite and the vermiculite samples, the low-TAC measurements reveal some C_p anomaly between 15 and 20 K (Fig. 4). For the vermiculite sample, the PPMS measurements do not show any anomaly, so that the broad peak obtained by low-TAC is probably an artefact due to desorption of He gas in the measurement cell. For the saponite sample, the anomaly is also probably due to an experimental artefact. Indeed, the probability of a magnetic ordering occurring at low temperature in a saponite with only very low Fe content is low, so that it seems unlikely that the anomaly would be associated with a magnetic transition of iron.

For the nontronite sample, a C_p anomaly, corresponding to an abnormal increase between 18 and 20 K, is observed by low-TAC. Moreover, complementary measurements between 2 K and 40 K carried out by PPMS both by heating and cooling successively, show a hysteresis associated with C_p values, between 3 and 18 K (Fig. 4). The origin of these anomalies is not known. In the following, the considered C_p values are those obtained by PPMS measured by heating from 2.3 K to 46 K, since they are in good agreement with low-TAC measurements (Fig. 4). However, the uncertainty on the C_p values associated with the hysteresis is taken into account for the estimation of the entropy uncertainty of the nontronite, which is assessed at 2.3% at 298.15 K.

Between 0 K and the lowest temperature measurements (8.06, 2.34 and 2.34 K, respectively for the Sap-Ca-1, the NAu-1 and the Santa Olalla vermiculite samples), the heat capacities are assessed using the Debye approximation, $C_p \approx C_v = \alpha T^3$, where C_v is the heat capacity at constant volume (Debye 1912). The corresponding C_p functions are given in Appendix 2.

Above the highest temperature attained by adiabatic calorimetry (377.98, 310.01 and 327.62 K, respectively, for the Sap-Ca-1, the NAu-1 and the Santa Olalla vermiculite), the heat

capacity values measured by DSC are fitted by the $C_p^0 = a_0 + a_1 T + a_2 T^{-2} + a_3 T^{-0.5}$ function using the least-squares method. By applying a suitable multiplying factor *k* (*k* = 1.030, 1.008 and 1.000, respectively for the Sap-Ca-1, the NAu-1 and the Santa Olalla vermiculite) due to calibration problems (Gailhanou et al. 2007), this function is fitted from the C_p value of the highest temperature reached by adiabatic calorimetry. The final modelled functions are given in Appendix 2. Relative errors for the least-squares fit method are lower than 0.75% for the Sap-Ca-1 and the Santa Olalla vermiculite samples and lower than 1.2% for the NAu-1. The scattering of the low-temperature measurements from PPMS is assessed for the vermiculite sample and is lower than 2% between 2 K and 50 K. For low-TAC measurements, the scattering decreases from 1% to 0.3% between 50 and 100 K and is lower than 0.3% above 100 K.

Heat capacities of the clay minerals. The heat capacities of the clay samples are linearly interpolated at every degree between 0 K and 520 K. The heat capacities of the clay minerals $C_{p,miner}{}^0$ are then obtained by subtracting the contribution of the impurities from the heat capacities of the samples, according to $C^0_{p,\,\mathrm{min}\,er} = \dfrac{C^0_{p,\,sample} - \sum_i x_i\, C^0_{p,\,i}}{x_{\mathrm{min}\,er}}$, where x_{miner} is the mass fraction of the mineral, $C_{p,sample}{}^0$ is the heat capacity of the sample, x_i and $C_{p,i}{}^0$ (in J/(K·g) are respectively the mass fraction (Table 3) and the heat capacity of the *i* impurity. The heat capacities of the clay minerals can then be calculated at any temperature. Molar heat capacity values, $C_{p,m}{}^0$, at selected temperatures for the three clay minerals are given in Tables 6-8.

The heat capacity data for the impurities are taken from the literature (see references in Appendix 3). In the case of goethite, the $C_p(T)$ curve of goethite presents an anomaly at about 375 K, associated with a magnetic Neel transition (Majzlan et al., 2003). Moreover, the heat capacity data for goethite are limited to 375 K as some dehydration occurs at higher

443 temperatures. Consequently, the correction of the heat capacity values of NAu-1 by
444 subtracting the contribution of the impurities is limited to 375 K.
445
446 **Heat contents**
447 The heat contents of minerals, $H^0(T) - H^0(298.15\ \mathrm{K})$, is calculated at any temperature by
448 integration of the $C_{p,m}{}^0$ function according to $H^0(T) - H^0(298.15K) = \int_{298.15}^{T} C_{p,m}^0 dT$ using the
449 trapezoid method at every degree (Tables 6-8).
450
451 **Entropy**
452 The third-law entropy of a mineral, $S°$, is expressed by $S^0 = S^{0(cal)} + S^{0(resid.)}$, with $S^{0(cal)}$ the
453 calorimetric entropy of the mineral and $S^{0(resid.)}$ the residual entropy, which is not available
454 from the calorimetric measurements and requires additional information about the mineral
455 (Ulbrich and Waldbaum 1976; Gailhanou et al. 2012).
456 **Calorimetric entropy.** The calorimetric entropy of a dehydrated mineral, for which
457 no phase change is observed, is determined by numerical integration with the trapezoid
458 method of the $\frac{C_{p,m}^0}{T}$ function at every degree according to $S^{0(cal)}(T) = \int_0^T \frac{C_{p,m}^0}{T} dT$ (numerical
459 integration with the trapezoid method, from the $\frac{C_{p,m}^0}{T}$ values at every degree).
460 **Chemical site configurational entropy.** The residual entropy may include several
461 contributions associated for example with chemical site disorder, isotopic mixing and
462 molecular disorder (Ulbrich and Waldbaum 1976). In particular, for clay minerals, the
463 chemical site configurational entropy, $S^{0(conf.)}$, is not negligible compared with the calorimetric
464 entropy and has to be assessed using additional structural information. This term is associated
465 with some chemical disorders inside the tetrahedral, octahedral and interlayer crystallographic

sites of the clay mineral, and consequently with the isomorphous substitutions of the cations in the sheets.

Several spectroscopic analyses and mechanistic calculations were investigated to provide information on the distribution of the cations in the octahedral layers (Cuadros et al. 1999; Sainz-Diaz et al. 2001; Sainz-Diaz et al. 2003; Drits et al. 2006), in the tetrahedral layers (Vinograd 1995) and in the interlayers (Iwasaki and Watanabe 1988). According to these results, the following criteria are applied for the distribution of the cations inside the layers and for estimating the entropic terms associated with the disorder in each type of layer (Gailhanou et al. 2012):

- Concerning the octahedral layer, the cations are randomly distributed in two octahedral sites, M1 and M2, for the trioctahedral clays, i.e. the saponite and the vermiculite. For the nontronite, the Al^{3+}, Fe^{3+} and Fe^{2+} cations are distributed among two octahedral sites, whereas Mg^{2+} is distributed in only one octahedral site, according to Gailhanou et al. (2012). This constraint was applied for dioctahedral smectites to avoid the formation of some Mg-OH-Mg pairs.
- For the tetrahedral layer, the entropic term is calculated in agreement with Vinograd's (1995) investigations for layer silicates. Thus, for the nontronite, among the distribution schemes suggested by the author, the homogeneous dispersion of the charge (HDC) model is considered with a Al/(Si+Al) ratio criterion of 0.11. The HDC model is in agreement with Loewenstein's rule of avoidance of Al-O-Al contact, and is more constraining since it includes some short-range restrictions to the second coordinational sphere of the honeycomb lattice. For the vermiculite, the HDC model is not suitable, since the Al/(Si+Al) ratio (r = 0.306) is higher than the criterion range for applying this model. Thus, the entropic term for the vermiculite is calculated using a third-degree polynomial function, obtained by fitting the experimental data from

Vinograd (1995) in the 0.20 – 0.308 range for the ratio *r*. The equation of the polynomial function for the tetrahedral configurational entropic term is $S^{0(conf.)}(r) = 4609.7\,r^3 - 4271.3r^2 + 1280r - 114.79$. For the saponite, which contains Si, Al and Fe^{3+} cations in tetrahedral layer, the statistical model of Vinograd (1995) is no longer suitable. Thus, the tetrahedral entropic term for the saponite is then estimated by taking into account the Al-avoidance rule only.

- The calculation of the entropic term for interlayers is the same as that described in Gailhanou et al. (2012) and is based on the Iwasaki and Watanabe (1988) studies on several smectites. The entropic term corresponds to an ideal entropy of mixing between sites occupied by a given cation (Ca, Na or K) and vacant sites. It assumes (i) a segregation of the different cations in the interlayers according to an interstratification of the Ca-smectite, the Na-smectite and/or the K-smectite layers, and (ii) an homogeneous interlayer charge of the smectite. This calculation is applied to the three clay minerals.

The chemical-site configurational entropies at 298 K for the three clay minerals are then obtained by summing the entropic terms associated with cation disorder in each type of layer. They are reported in Table 11.

Estimated uncertainties on entropy. The estimate of uncertainties associated with entropy values is limited to uncertainties on calorimetric entropies, due to our lack of knowledge for estimating uncertainties on configurational entropies.

Uncertainties are calculated by considering maximum uncertainties estimated for C_p^0 values, including both accuracy and scattering contributions, measured on the standard reference material SRM 720 (synthetic sapphire). The estimated uncertainties on entropies are maximum values and should be considered as qualitative rather than quantitative values.

515 However, these estimates are not impacting too significantly the final uncertainties on ΔG_f^0
516 for clay minerals, since the uncertainties on entropies contribute less than those on ΔH_f^0.
517
518 **Enthalpies of formation**
519 **Enthalpies of dissolution at 298.15 K.** The solution enthalpies of the clay samples
520 $\Delta H_{diss,sample}$ and the solution enthalpies of the mixture of secondary references (except for
521 H_2O) $\Delta H_{diss,mixt.}$ in HF-HNO_3 solutions are given in Table 9. The enthalpies of dilution ΔH_{dil}
522 are respectively, -2.57 (± 0.13) kJ/mol in HF(6M) – HNO_3(7M) and -3.69 (± 0.12) kJ/mol in
523 HF(3M) – HNO_3(10M). The former solution is used for the experiments on the Sap-Ca-1 and
524 the NAu-1 samples, whereas the latter solution is used for the experiments on the Santa Olalla
525 vermiculite sample. Moreover, for the experiments on the nontronite NAu-1, involving
526 HNO_3, the solution enthalpies ΔH_{sol} associated with the mixing of pure HNO_3 in HF(6M) -
527 HNO_3(7M) solution is approximated at 2.57 kJ/mol (± 4.50), which is the value measured for
528 ΔH_{sol} in HF(10M) - HNO_3(6M), in the case of the beidellite SBId-1 study (Gailhanou et al.
529 2012). This assumption is justified by the fact that the measurement of ΔH_{sol} in the
530 appropriate concentration range is too difficult to be performed, due to the too low amount of
531 HNO_3 necessary for equilibrating the reaction of formation of the nontronite from the
532 constituents (Table 10). Anyway, in this case, the term $n_{HNO3}*\Delta H_{sol}$ is negligible compared to
533 the other terms of the equation (1).
534 The uncertainties associated with the mean enthalpies of dissolution and dilution are
535 calculated from the measured values using Student's t-distribution with a 95% confidence
536 interval.
537 **Enthalpies of formation from the secondary reference constituents.** The enthalpies
538 of formation from the secondary reference constituents are calculated using the relation (1)

and are given in Table 10. The values of the parameters and the reactions of formation of the clay minerals from the secondary reference constituents are also given in Table 10.

Uncertainties on these enthalpies of formation have been obtained by using a classical error propagation method, notably described in Ellison et al. (2000). These standard uncertainties correspond to one standard deviation.

In the following, the same error propagation method has been used for properties resulting from combinations. This applies notably to the standard formation enthalpy and Gibbs free energy of formation of the minerals.

Standard enthalpies of formation. The standard enthalpies of formation of clay minerals at 298.15 K (Table 11) are obtained from the enthalpies of formation of minerals from the secondary reference constituents and from the standard enthalpies of formation of these reference constituents at 298.15 K. These latter values are given in Appendix 1.

The uncertainties associated with ΔH_f^0 are calculated according to:

$$\Delta(\Delta H_f^0) = \sqrt{\Delta(\Delta H_{f/contit.}^0)^2 + \sum_i \nu_i^2 \, \Delta(\Delta H_f^{constit.i})^2},$$

where ν_i and $\Delta H_f^{constit.i}$ are respectively the stoichiometric coefficient and the standard enthalpy of formation associated with the constituent *i*. These standard uncertainties correspond to one standard deviation.

Thermodynamic datasets of minerals

The complete thermodynamic datasets of the dehydrated and hydrated clay minerals are provided in Table 11.

The standard entropies of formation of the clay minerals at 298.15 K, ΔS_f^0, are determined from the entropies of the clays and the entropies of the elements in their standard reference state (Appendix 4). Finally, the standard Gibbs free energies of formation of the clay minerals

563 at 298.15 K are calculated according to
564 $\Delta G_f^0(298.15K) = \Delta H_f^0(298.15K) - 298.15\,\Delta S_f^0(298.15K)$.

565 **DISCUSSION**

566 The present calorimetric study provides the thermodynamic properties of nontronite, saponite
567 and vermiculite. The assessment of these data could be done with respect to previous
568 experimental works and/or with respect to field observations. From these latter, a
569 methodology would be to build predominance diagrams including the minerals whose
570 properties had been measured in the present work and compare the stability domains with
571 field observations. However, this kind of verification is limited in the case of clay minerals
572 due to their multi-elemental composition; their stability has to be considered in large chemical
573 systems which are difficult to reduce to a 2D representation (or even 3D). The three mineral
574 presented here are composed by seven to nine chemical elements (or six to eight elements for
575 their simplified structural formulae), apart from O and H. Using predominance diagram in a
576 2D representation would require to fix the activity of four to six elements in the chemical
577 system. We have experimented difficulties in finding a consensual set of constraints for this
578 complex operation.
579 Moreover, we have tried to find experimental works where equilibration experiments with
580 either nontronite or vermiculite or saponite were performed. For nontronite, to our
581 knowledge, none could be found in literature. For vermiculite, hydrothermal experiments
582 were conducted by Roy and Romo (1957) between 150°C and 750°C at 694 bars and by
583 Mosser-Ruck et al. (2003) between 150°C and 300°C at 75 and 100 bars. Roy and Romo
584 (1957) observed the transformation of vermiculite into a “pseudo-chlorite” (probably a
585 smectite-chlorite or chlorite-vermiculite), and Mösser-Ruck (2003) observed its
586 transformation into a mixed-layered saponite-chlorite. For saponite, the assessment of data
587 has been performed by using Whitney’s (1983) work. The authors performed hydrothermal

588 syntheses from gels, at 1kbars and between 300 and 550°C and could observe, depending on
589 the experimental conditions, the precipitation of sodic saponites and, at higher temperature,
590 the precipitation of saponite/talc interstratified minerals. We have considered that the lowest
591 temperature for talc appearance could be approximated as the Na-saponite/talc transition
592 temperature (400°C). From these experimental results, we have then tried to assess our data
593 by calculating the Gibbs free energies of the reaction of transformation of the vermiculite
594 Santa Ollala into a clinochlore, based on a conservative number of twelve oxygen atoms per
595 unit formula, between 25 and 500°C, and the Gibbs free energy of the transformation of Na-
596 saponite Sap-Ca-1 into talc, for 1 mole of each, at 1 kbars, between 25 and 500°C. The
597 transition temperatures calculated don't seem inconsistent with regards to experimental
598 observations, with a difference of about 50°C for saponite-talc and about 150°C for
599 vermiculite-chlorite transformations. However, the reliability of these results must be
600 questioned because, in the previous experimental studies, the chemical compositions of most
601 of minerals as well as the equations of chemical reactions are unknown. Finally, our attempt
602 to assess the reliability of thermodynamic data of clay minerals aims above all in showing the
603 complexity of this exercise for a clay mineral, compared with a compound with a fixed
604 composition.
605 To date, very few thermodynamic properties have been directly measured for 2:1 clay
606 minerals except for the work of Gailhanou et al. (2012) on illite, smectite and beidellite and
607 for equilibrium constants from solution experiments. The situation is even worse for ferro-
608 magnesian minerals. Up to now, estimation methods have remained the only source of
609 thermodynamic data for such minerals. It seems interesting to test the results of some
610 estimation methods against the set of experimental measurements acquired by Gailhanou et
611 al. (2012) and in this work. Estimation methods offer the opportunity to consider a wide range
612 of clay mineral compositions, provided the estimates remain accurate. The aim of the present

comparison is to test this accuracy. A similar exercise has been proposed by Gailhanou et al. (2012) for three aluminous clay minerals. The present measurements allow the range of the comparison to be extended to ferro-magnesian and high charge 2:1 clay minerals.

Only a few of the predictive methods available in the literature were selected for the present analysis, among the most popular or recent ones. For ΔG^0_f, both the models of Chermak and Rimstidt (1989) and Vieillard (2002) were used, whereas for ΔH^0_f, only the polyhedral decomposition method of Chermak and Rimstidt (1989) was considered. For predicting entropy values, the model from Holland (1989) was retained, together with the Berman and Brown (1985) method for the heat capacity prediction. The comparison is illustrated in Figures 5 to 9.

In these estimation methods, some minor elements, such as Mn and Ti, are not taken into account due to their low occurrences in silicates and phyllosilicates. In the case of the three studied clay minerals, low amounts of Mn and/or Ti are present in the clay structures. The estimation methods are then applied on simplified structural formulae, obtained by substituting arbitrarily Mn and/or Ti cations by other cations present in the structure. The following fictive reactions were considered for saponite Sap-Ca-1, nontronite NAu-1 and Santa Olalla vermiculite:

- Saponite:

$Na_{0.394}K_{0.021}Ca_{0.038}(Si_{3.569}Al_{0.397}Fe^{3+}_{0.034})(Mg_{2.948}Fe^{2+}_{0.021}Mn_{0.001})O_{10}(OH)_2 + 0.001\ MgO =$
$Na_{0.394}K_{0.021}Ca_{0.038}(Si_{3.569}Al_{0.397}Fe^{3+}_{0.034})(Mg_{2.949}Fe^{2+}_{0.021})O_{10}(OH)_2 + 0.001\ MnO$

- Nontronite:

$Ca_{0.247}K_{0.020}(Si_{3.458}Al_{0.542})(Al_{0.268}Mg_{0.066}Fe^{3+}_{1.688}Ti_{0.007})O_{10}(OH)_2 + 0.004\ Al_2O_3 + 0.002\ MgO$
$= Ca_{0.247}K_{0.020}(Si_{3.458}Al_{0.542})(Fe^{3+}_{1.688}Al_{0.276}Mg_{0.068})O_{10}(OH)_2 + 0.007\ TiO_2$

- vermiculite:

637 $Ca_{0.445}(Si_{2.778}Al_{1.222})(Al_{0.192}Mg_{2.468}Fe^{3+}_{0.226}Fe^{2+}_{0.028}Ti_{0.018}Mn_{0.007})O_{10}(OH)_2$ + 0.012 Al_2O_3 +
638 0.007 MgO = $Ca_{0.445}(Si_{2.778}Al_{1.222})(Al_{0.216}Mg_{2.475}Fe^{3+}_{0.226}Fe^{2+}_{0.028})O_{10}(OH)_2$ + 0.018 TiO_2 +
639 0.007 MnO

640 The assessment of the predictive methods is then carried out by comparing estimated values
641 with the experimental derived thermodynamic data associated with the modified compositions
642 of clay minerals (Table 11). These are calculated by assuming the energies of reaction ($\Delta G_r°$,
643 $\Delta H_r°$, $\Delta S_r°$ at 298.15 K and $\Delta C_{p,r}$ between 298.15 K and 500 K) to be zero. The
644 thermodynamic data for oxides are given in Appendix 5.

645 For ΔG_f^0 and ΔH_f^0 estimates, Figures 5 and 6 illustrate the tendency of the Chermak and
646 Rimstidt (1989) method to overestimate the stability of clay minerals. This tendency is
647 stronger for the ΔH_f^0 estimate. For smectites and illite, the discrepancy ranges from 10 to 30
648 kJ/mol. However, it dramatically increases for nontronite and vermiculite. This underlines the
649 problem of constraining the ferric contribution, a point already discussed by Chermak and
650 Rimstidt (1989). In addition, the unexpected results obtained on vermiculite indicate a
651 problem in predicting the properties of clay minerals having a high degree of tetrahedral
652 substitution. The problem begins to appear with illite (tetrahedral composition of $Si_{3.385}Al_{0.615}$
653 per $O_{10}(OH)_2$, discrepancy of 16 kJ/mol for ΔG_f^0) and it develops with vermiculite (tetrahedral
654 composition of $Si_{2.778}Al_{1.222}$ per $O_{10}(OH)_2$, discrepancy of 74 kJ/mol for ΔG_f^0). Globally, the
655 range of discrepancies is different for ΔG_f^0 or ΔH_f^0 estimates, indicating a consistency
656 problem in the Chermak and Rimstidt (1989) method, which was already suspected by
657 Gailhanou et al. (2012) and is confirmed here. For the Vieillard (2002) method (Fig. 6),
658 overall, it displays a smaller scattering of the discrepancies with respect to experimental data.
659 However, the same tendency appears, which is a global overestimation of ΔG_f^0, especially for
660 nontronite and vermiculite.

Considering the case of entropy, Figure 7 compares the experimental values to those estimated from the Holland (1989) method. The results reported indicate a systematic underestimate of the entropy by 36 J/(K·mol). This systematic discrepancy was already suspected by Gailhanou et al. (2012). The data measured here enable this to be confirmed and to clarify the extent of the underestimate. Figures 8 and 9 report the results obtained on $C_p^0(T)$ estimates, at 25 °C for Figure 8 and as a function of temperature for Figure 9. From Figure 8, it appears that heat capacities predicted by the method of Berman and Brown (1985) suffer from a small, systematic underestimation by about 10 J/(K·mol) at 25 °C. Figure 8 shows that the underestimates of the heat capacity globally increase for high temperatures.

Finally, it appears that certain calculation methods could provide some estimates for smectites and illites, in spite of discrepancy and consistency problems. However, the problems become unacceptable for Fe(III) rich minerals or minerals displaying a high degree of tetrahedral substitution. The present work proposes data that could help to improve the parameterization of predictive methods for the thermodynamic properties of clay minerals.

Anyway, the thermodynamic properties measured in the present work for clay minerals are reference data since they were obtained by calorimetric methods, independently from a solution equilibrium. By this way, those data don't depend on the equilibrium state attainment, which is generally rather long for silicates (Rimstidt 1997), and they are especially relevant for long-term applications, e.g. in contexts such as deep disposal applications.

Modelling the geochemical behaviour of clays over shorter periods of times may require to consider additionally the kinetics of the mineral transformations. In particular, the dissolution mechanisms of clay phases are controlled by the surface reactivity of clays, including notably surface complexation reactions (Bradbury and Baeyens 2009), which have to be considered in addition to the thermodynamic stability of the phases.

686

687

688 **ACKNOWLEDGEMENTS**

689 We are very grateful to Jan Srodon and Luis A. Pérez-Maqueda for their kindness in
690 providing us with clay samples for this study, and Susana Ramirez and Stephane Gaboreau
691 for their help in the search for the vermiculite sample. Financial support from the French
692 National Radioactive Waste Management Agency (ANDRA), and from the French
693 Geological Survey (BRGM) is gratefully acknowledged. We thank Laurent Truche and the
694 anonymous reviewers for their meaningful remarks, which have helped us to improve the
695 quality of the manuscript.

696

697

698

699 **REFERENCES CITED**

700 Argüelles, A., Leoni, M., Blanco, J.A., and Marcos, C. (2010) Semi-ordered crystalline
701 structure of the Santa Olalla vermiculite inferred from X-ray powder diffraction.
702 American Mineralogist, 95, 126-134.

703 Atake, T., Kawaji, H., Hamano, A., and Saito, Y. (1990) Report of the Research Laboratory
704 of Engineering Materials. Tokyo Institute of Technology 15, p13.

705 Bergaoui, L., Lambert, J.E., Vicente-Rodriguez, M.A., Michot, .L.J., and Villiéras, F. (1995)
706 Porosity of synthetic saponites with variable layer charge pillared by Al_{13} polycations.
707 Langmuir, 11, 2849-2852.

708 Berman, R.G. and Brown, T.H. (1985) Heat capacity of minerals in the system Na_2O-K_2O-
709 CaO-MgO-FeO-Fe_2O_3-Al_2O_3-SiO_2-TiO_2-H_2O-CO_2: representation, estimation and high
710 temperature extrapolation. Contribution to Mineralogy and Petrolology, 89, 168-183.

711 Blanc, P., Legendre, O., and Gaucher, E.C. (2007) Estimate of clay minerals amounts from
712 XRD pattern modeling: The Arquant model. Physics and Chemistry of the Earth, 32,
713 135–144.

714 Bradbury, M.H. and Baeyens, B. (2009) Experimental and modelling studies on the pH
715 buffering of MX-80 bentonite porewater. Applied Geochemistry, 24, 419-425.

716 Charpentier, D., Devineau, K., Mosser-Ruck, R., Cathelineau, M., and Villiéras, F. (2006)
717 Bentonite-iron interactions under alkaline condition: an experimental approach. Applied
718 Clay Sciences, 32, 1-13.

719 Chermak, J.A. and Rimstidt, J.D. (1989) Estimating the thermodynamic properties (ΔG_f^0 and
720 ΔH_f^0) of silicate minerals at 298 K from the sum of polyhedral contributions. American
721 Mineralogist, 74, 1023–1031.

722 Cuadros, J., Sainz-Diaz, C., Ramirez, R., and Hernández-Laguna, A. (1999) Analysis of Fe
723 segregation in the octahedral sheet of bentonitic illite-smectite by means of FT-IR, ^{27}Al

MAS NMR and reverse Monte Carlo simulations. American Journal of Sciences, 299, 289-308.

Cuevas, J. (2005) Geochemical reactions in FEBEX bentonite. In, Andra (2005). Ecoclay II: Effects of Cement on Clay Barrier Performance – Phase II. Final Report. EC Project No. FIKW-CT-2000-00028; Andra Report No. CRPASCM04-0009, 103-115.

Dachs, E. and Bertoldi, C. (2005) Precision and accuracy of the heat-pulse calorimetric technique : low-temperature heat capacities of milligram-sized synthetic mineral samples. European Journal of Mineralogy, 17, 251-261.

de la Calle, C. (1977) Structure des Vermiculites. Facteurs conditionnant les mouvements des feuillets. Ph.D. thesis, Université Paris VI, France.

Ditmars, D.A., Ishihara, S., Chang, S.S., and Bernstein, G. (1982) Enthalpy and heat-capacity standard reference material: synthetic sapphire (α-Al_2O_3) from 10 to 2250 K. Journal of Research of the National Bureau of Standards, 87, 159–163.

Drits, V.A. and Tchoubar, C. (1990) X-ray Diffraction by Disordered Lamellar Structures. Springer-Verlag, Berlin.

Drits, V.A., McCarty, D., and Zviagina, B.B. (2006) Crystal-chemical factors responsible for the distribution of octahedral cations over trans- and cis-sites in dioctahedral 2:1 layer silicates. Clays and Clay Minerals, 54, 131-152.

Ellison, S.L.R., Roesslein, M, and Williams, A. (Eds.). (2000) EURACHEM/CITAC Guide: quantifying uncertainty in analytical measurement, 2nd ed. EURACHEM. ISBN 0-948926-15-5.

Gailhanou, H., van Miltenburg, J.C., Rogez, J., Olives, J., Amouric, A., Gaucher, E.C., and Blanc, P. (2007) Thermodynamic properties of anhydrous smectite MX-80, illite IMt-2, and mixed-layer illite-smectite ISCz-1 as determined by calorimetric methods: Part I.

748 Heat capacities, heat contents and entropies. Geochimica et Cosmochimica Acta, 71,
749 5463–5473.
750 Gailhanou, H., Rogez, J., van Miltenburg, J.C., van Genderen, A.C.G., Grenèche, J.M., Gilles,
751 C., Jalabert, D., Michau, N., Gaucher, E.C., and Blanc, P. (2009) Thermodynamic
752 properties of chlorite CCa-2. Heat capacities, heat contents and entropies. Geochimica et
753 Cosmochimica Acta, 73, 4738–4749.
754 Gailhanou, H., Blanc, P., Rogez, J., Mikaelian, G., Kawaji, H., Olives, J., Amouric, M.,
755 Denoyel, R., Bourrelly, S., Montouillout, V., Vieillard, P., Fialips, C.I., Michau, N., and
756 Gaucher, E.C. (2012) Thermodynamic properties of illite, smectite and beidellite by
757 calorimetric methods: enthalpies of formation, heat capacities, entropies and Gibbs free
758 energies of formation. Geochimica et Cosmochimica Acta., 89, 279–301.
759 Ganteaume, M., Coten, M., and Decressac, M. (1991) Un nouveau calorimètre en solution : le
760 Calsol. Thermochimica Acta, 178, 81-98.
761 Gaucher, E.C. and Blanc, P. (2006) Cement/clay interactions – A review : Experiments,
762 natural analogues, and modeling. Waste Management, 26, 776-788.
763 Gaucher, E.C., Blanc, P., Matray, J.-M., and Michau, N. (2004) Modeling diffusion of an
764 alkaline plume in a clay barrier. Applied Geochemistry, 19, 1505-1515.
765 Gournis, D., Lappas, A., Karakassides, M.A., Többens, D., and Moukarika, A. (2008) A
766 neutron diffraction study of alkali cation migration in montmorillonites. Physics and
767 Chemistry of Minerals, 35, 49-58.
768 Guillaume, D., Neaman, A., Cathelineau, M., Mosser-Ruck, R., Peiffert, C., Abdelmoula, M.,
769 Dubessy, F., Villiéras, F., and Michau, N. (2004) Experimental study of the
770 transformation of smectite at 80 °C and 300 °C in the presence of Fe oxides. Clay
771 Minerals, 39, 17–34.

772 Hillier, S. (2000) Accurate quantitative analysis of clay and other minerals in sandstones by
773 XRD: comparison of a Rietveld and a reference intensity ratio (RIR) method and the
774 importance of sample preparation. Clay Minerals, 35, 291–302.
775 Holland, T.J.B. (1989) Dependence of entropy on volume for silicate and oxide minerals: A
776 review and a predictive model. American Mineralogist, 74, 5-13.
777 Iwasaki, T. and Watanabe, T. (1988) Distribution of Ca and Na ions in dioctahedral smectites
778 and interstratified dioctahedral mica/smectites. Clays and Clay Minerals, 36, 73-82.
779 Johnson, G.K., Tasker, I.R., Flotow, H.E., and O'Hare, P.A.G. (1992) Thermodynamic studies
780 of mordenite, dehydrated mordenite and gibbsite. American Mineralogist, 77, 85-93.
781 Kalinowski, B.E. and Schweda, P. (2007) Rates and nonstoichiometry of vermiculite
782 dissolution at 22°C. Geoderma, 142, 197-209.
783 Keeling, J.L., Raven, M.D., and Gates, W.P. (2000) Geology and characterization of two
784 hydrothermal nontronites from weathered metamorphic rocks at the Uley graphite mine,
785 South Australia. Clays and Clay Minerals, 48, 537-548.
786 Kraus, W. and Nolze, G. (2000) Powder Cell for Windows version 2.4. Federal Institute for
787 Materials Research and Testing, Rudower Chaussee 5, Berlin GE, 2000.
788 Lantenois, S., Lanson, B., Muller, F., Bauer, A., Jullien, M., and Plançon, A. (2005)
789 Experimental study of smectite interaction with metal Fe at low temperature: 1. Smectite
790 destabilization. Clays and Clay Minerals, 53, 597–612.
791 Majzlan, J., Lang, B.E., Stevens, R., Navrotsky, A., Woodfield, B.F., and Boerio-Goates, J.
792 (2003) Thermodynamics of Fe oxides: Part I. Entropy at standard temperature and
793 pressure and heat capacity of goethite (α-FeOOH), lepidocrocite (γ-FeOOH), and
794 maghemite (γ-Fe_2O_3). American Mineralogist, 88, 846-854.
795 Manceau, A., Chateigner, D., and Gates, W.P. (1998) Polarized EXAFS, distance-valence
796 least-squares modeling (DLVS), and quantitative texture analysis approaches to the

structural refinement of Garfield nontronite. Physics and Chemistry of Minerals, 25, 347-365.

Mehra, O.P. and Jackson, M.L. (1958) Iron oxide removal from soils and clays by a dithionite-citrate system buffered with sodium bicarbonate. Clays and Clay Minerals, 7, 317-327.

Mosser-Ruck, R., Pironon, J., Guillaume, D, and Cathelineau, M. (2003) Experimental alteration of Mg-vermiculite under hydrothermal conditions: formation of mixed-layered saponite-chlorite minerals. Clay Minerals, 38, 303–314.

Mosser-Ruck, R., Cathelineau, M., Guillaume, D., Charpentier, D., Rousset, D., Barres, O., and Michau, N. (2010) Effects of temperature, pH, and iron/clay and liquid/clay ratios on Experimental Conversion of Dioctahedral Smectite To Berthierine, Chlorite, Vermiculite or Saponite. Clays and Clay minerals, 58, 280-291.

Nagy, K., Schlegel, M., Cheng, L., Fenter, P., and Sturchio, N. (2000) Alteration of Muscovite to a Mg-Clay. Goldschmidt Conference 2000, Journal of Conference Abstracts, 5, p. 737.

Norrish, K. (1973) Factors in the weathering of mica to vermiculite: in Proc. Int. Clay Conf., Madrid, 1972, J. M. Serratosa, ed., Div. Ciencias, C.S.I.C., Madrid, 417-432.

Pérez-Maqueda, L.A., Caneo, O.B., Poyato, J., and Pérez-Rodriguez, J.L. (2001) Preparation and characterization of micron and submicron-sized vermiculite. Physics and Chemistry of Minerals, 28, 61-66.

Post, J.L. (1984) Saponite from near Ballarat, California. Clays and Clay Minerals, 32, 147-153.

Pouchou, J.L. and Pichouar, F. (1984) Un nouveau modèle de calcul pour la microanalyse quantitative par spectrométrie de rayon X. Partie 1: application a` l'analyse d'échantillons homogènes. La recherche Aérospatiale, 3, 167–192.

822 Reynolds, R.C. (1985) A computer program for the calculation of one-dimensional diffraction
823 pattern of mixed-layer clays. R.C. Reynolds, 8 Brook RD., Hanover, NH 03755, USA.
824 Rimstidt, D.J. (1997) Quartz solubility at low temperatures. Geochimica et Cosmochimica
825 Acta, 61, 2553-2558.
826 Roy, R. and Romo, L. A. (1957) Weathering Studies. 1. New Data on Vermiculite. Journal of
827 Geology, 65, 603–610.
828 Sainz-Diaz, C.I., Cuadros, J., and Hernández-Laguna, A. (2001) Cation distribution in the
829 octahedral sheet of dioctahedral 2:1 phyllosilicates by using inverse Monte Carlo
830 methods. Physics and Chemistry of Minerals, 28, 445-454.
831 Sainz-Diaz, C.I., Palin, E.J., Dove, M.T., and Hernández-Laguna, A. (2003) Monte Carlo
832 simulations of ordering of Al, Fe, and Mg cations in the octahedral sheet of smectites
833 and illites. American Mineralogist, 88, 1033-1045.
834 Savage, D., Noy, D., and Mihara, M. (2002) Modeling the interaction of bentonite with
835 hyperalkaline fluids. Applied Geochemistry, 17, 207-223.
836 Shirozu, H. and Bailey, S.W. (1966) Crystal structure of a two-layer Mg-vermiculite.
837 American Mineralogist, 51, 1124-1143.
838 Stølen, S. and Grønvold, F. (1999) Review critical assessment of the enthalpy of fusion of
839 metals used as enthalpy standards at moderate to high temperatures. Thermochimica
840 Acta, 327, 1–32.
841 Suquet, H. and Pezerat, H. (1987) Parameters influencing layer stacking types in saponite and
842 vermiculite: a review. Clays and Clay Minerals, 35, 353-362.
843 Toranzo, R., Vicente, M.A., Banares-Munoz, M.A., Gandia, L.M., and Gil, A. (1998)
844 Pillaring of saponite with zirconium oligomers. Microporous and Mesoporous Materials,
845 24,173-188.

Ulbrich, H.H. and Waldbaum, D.R. (1976) Structural and other contributions to the third-law entropies of silicates. Geochimica et Cosmochimica Acta, 40, 1–24.

Vieillard, P. (2002) A new method for the prediction of Gibbs free energies of formation of phyllosilicates (10Å and 14Å) based on the electronegativity scale. Clays and Clay Minerals, 50, 352–363.

Vinograd, V.L. (1995) Substitution of $^{[4]}$Al in Layer Silicates: Calculation of the AI-Si Configurational Entropy according to ^{29}Si NMR Spectra. Physics and Chemistry of Minerals, 22, 87-98.

Whitney, G. (1983) Hydrothermal reactivity of saponite. Clays and Clay Minerals, 31, 1–8.

Wilson, J., Cressey, G., Cressey, B., Cuadros, J., Ragnarsdottir, K., Savage, D., and Shibata, M. (2006) The effect of iron on montmorillonite stability. (II) Experimental investigation. Geochimica et Cosmochimica Acta, 70, 323–336.

Yamamura, Y., Saito, K., Saitoh, H., Matsuyama, H., Kikuchi, K., and Ikemoto, I. (1995) Heat capacity measurements and phase transition of crystalline 4,4-difluoro-p-terphenyl. Journal of Physics and Chemistry of Solids, 56, 107-115.

862 **FIGURE CAPTIONS**

863

864 Figure 1. Statistical treatment by the PCA method of the microprobe analyses of (a)
865 saponite Sap-Ca-1, (b) nontronite NAu-1 and (c) Santa Olalla vermiculite. Biplot
866 representations of individuals and variables onto plans defined by the eigenvectors ($\mathbf{F_1}$, $\mathbf{F_2}$).

867 Figure 2. ^{57}Fe Mössbauer spectrum at 77 K for the nontronite Nau-1 sample (in red,
868 magnetic component for Fe^{3+} in goethite; in blue, component for Fe^{3+} in nontronite).

869 Figure 3. TGA curves for the powdered Ca-vermiculite from Santa Olalla.
870 Temperature dependence of the weight loss (solid line) and the derivative of weight loss
871 versus temperature (dashed line) showing two peaks at 90 °C and 185 °C.

872 Figure 4. Measured heat capacities of samples (including impurities) (a) saponite Sap-
873 Ca-1; (b) nontronite NAu-1; (c) Santa Olalla vermiculite. (Circles: low-TAC; up triangles:
874 DSC; crosses: PPMS by heating; black diamonds: PPMS by cooling).

875 Figure 5. Discrepancy between experimental and predicted values of the Gibbs free
876 energy $\Delta(\Delta G^0_f)$ and the enthalpy of formation $\Delta(\Delta H^0_f)$ of 6 clay minerals, at 298.15 K and 1
877 bar. Experimental measurements are from Gailhanou et al. (2012) for the smectite MX80, the
878 illite IMt-2 and the beidellite SBId-1. For the nontronite NAu-1, the Santa Olalla vermiculite
879 (vermiculite SO) and the saponite SapCa-1, the experimental values are obtained in this work.
880 The estimate of ΔG^0_f and ΔH^0_f are calculated using the Chermak and Rimstidt (1989) method.
881 The dotted lines represent an uncertainty interval that could correspond to 1 unit on the 25°C
882 Log*K* equilibrium constant.

883 Figure 6. Discrepancy between experimental and predicted values of the Gibbs free
884 energy $\Delta(\Delta G^0_f)$ for 6 clay minerals, at 298.15 K and 1 bar. Experimental values have the same
885 origin as in Figure 5. The estimates of ΔG^0_f are calculated using the Vieillard (2002) and the

886 Chermak and Rimstidt (1989) methods. The dotted lines are defined in the same way as in
887 Figure 5.

888 Figure 7. Comparison between experimental and predicted values of the standard
889 entropy of 6 clay minerals, hydrated and dehydrated, at 298.15 K and 1 bar. Experimental
890 measurements are from Gailhanou et al. (2007, 2012) for smectite MX80, illite IMt-2 and
891 beidellite SBId-1. For nontronite NAu-1, Santa Olalla vermiculite and saponite SapCa-1, the
892 experimental values are obtained in this work. The estimates of S^0 are calculated using the
893 Holland (1989) method.

894 Figure 8. Comparison between experimental and predicted values of the $C_p°$(298.15
895 K) of 6 clay minerals, hydrated and dehydrated. Experimental measurements have the same
896 origin as in Figure 9. The estimates of $C_p°$(298.15 K) are calculated using the Berman and
897 Brown (1985) method.

898 Figure 9. Discrepancy ($\Delta C_p(T)$) between experimental and predicted values of the
899 $C_p°(T)$ function for 6 clay minerals. Experimental measurements have the same origin as in
900 Figure 9. The estimate of the $C_p°(T)$ function are calculated using the Berman and Brown
901 (1985) method.

902

903

904

905

APPENDICES

Appendix 1. Standard enthalpies of formation at 298.15 K of the constituents used for solution calorimetry experiments.

Appendix 2. Heat capacity raw data measured on saponite Sap-Ca-1, nontronite NAu-1 and Santa Olalla vermiculite samples.

Appendix 3. References for heat capacity data of mineral impurities.

Appendix 4. Standard entropies of elements in their reference state at 298.15 K.

Appendix 5. Thermodynamic data of oxides used for estimating the thermodynamic properties of the modified compositions of clay minerals.

917 **TABLES**
918

919 Table 1. Chemical compositions (wt%) of the samples at ambient RH

	Saponite Sap-Ca-1	Nontronite NAu-1	Santa Olalla vermiculite	Analytical techniques
$C_{mineral}$	< 0.05	0.05	< 0.05	(a)
C_{total}	0.09	0.05	0.42	(b)
S_{total}	0.01	< 0.01	0.02	(b)
SiO_2	49.15	42.10	35.20	(c)
Al_2O_3	4.60	10.20	15.00	(c)
FeO	0.34	n.d.*	0.42	(d)
Fe_2O_3	0.59	27.10	3.76	(c,d)
CaO	0.90	2.60	5.20	(c)
MgO	26.8	0.50	20.70	(c)
MnO	0.03	< 0.02	0.11	(c)
K_2O	0.25	0.17	< 0.05	(c)
Na_2O	2.70	< 0.20	< 0.20	(c)
TiO_2	0.24	0.11	0.30	(c)
P_2O_5	< 0.05	0.05	< 0.05	(c)
L.O.I. (Loss on ignition)	13.90	16.70	19.80	(e)
Total	99.60	99.58	100.93	(e)

Note: (a) volumetric method, (b) infra-red spectroscopy, (c) X-ray fluorescence, (d) volumetric titration and (e) weight loss while heating up to 1000°C.
The relative uncertainties on the presented results are estimated to be 2%.
* n.d.: not detected by ^{57}Fe Mössbauer spectrometry.

920

921 Table 2. ^{57}Fe Mössbauer parameters obtained from modelling of the spectrum at 77 K
922 acquired for the nontronite Nau-1 sample.

Mineral		Isomer shift (mm/s) ± 0.02	Width (mm/s) ± 0.02	Quadrupolar shift or quadrupolar splitting (mm/s) ± 0.01	Magnetic field (T) ± 0.5	Fe content (%) ± 2
Goethite	Fe^{3+}	0.51	0.50	-0.20	49.7	6
Goethite	Fe^{3+}	0.51	0.50	-0.20	47.3	6
Nontronite	Fe^{3+} (in octahedral coordination)	0.46	0.60	0.83		48
Nontronite	Fe^{3+} (in octahedral coordination)	0.45	0.54	0.27		39

923

924 Table 3. Amounts of impurities (wt%) in the samples at ambient RH and in dehydrated states.

	Quartz	Cristobalite	Muscovite	Diopside	Tremolite	Kaolinite	TiO_2 oxide	Goethite
At ambient RH								
Saponite Sap-Ca-1	0.25		0.3	1	1.25		0.24†	
Nontronite NAu-1	0.2					6.2		2.0
Santa Olalla vermiculite	0.3	0.15						
Dehydrated samples*								
Saponite Sap-Ca-1	0.28		0.33	1.11	1.38		0.27	
Nontronite NAu-1	0.2					7.1		2.3
Santa Olalla vermiculite	0.35	0.18						

Note: * Calculated from the amounts at ambient RH by removing the amount of molecular water from the total mass of the samples
† From the chemical analyses.

925

926

927 Table 4. Structural formulae and molar masses of the dehydrated clay minerals

	Formula	Molar mass (g/mol)
Saponite Sap-Ca-1	$Na_{0.394}K_{0.021}Ca_{0.038}(Si_{3.569}Al_{0.397}Fe^{3+}_{0.034})(Mg_{2.948}Fe^{2+}_{0.021}Mn_{0.001})O_{10}(OH)_2$	391.15
Nontronite NAu-1	$Ca_{0.247}K_{0.020}(Si_{3.458}Al_{0.542})(Mg_{0.066}Fe^{3+}_{1.688}Al_{0.268}Ti_{0.007})O_{10}(OH)_2$	419.84
Santa Olalla vermiculite	$Ca_{0.445}(Si_{2.778}Al_{1.222})(Al_{0.192}Mg_{2.468}Fe^{3+}_{0.226}Fe^{2+}_{0.028}Ti_{0.018}Mn_{0.007})O_{10}(OH)_2$	403.46

928

929

930

931

932

933

934 Table 5. Molar volumes and cell parameters determined from XRD analyses

Name	*a* (Å)	*b* (Å)	*c* (Å)	$V°$ (cm^3/mol)
		Dehydrated		
Saponite SapCa-1	5.31	9.19	9.76	141.66
Nontronite Nau-1	5.27	9.13	9.76	136.38
Santa Olalla vermiculite	5.36	9.28	10.07	148.36
		Ambient RH		
Saponite SapCa-1	5.31	9.19	12.67	183.97
Nontronite Nau-1	5.27	9.13	15.34	214.24
Santa Olalla vermiculite	5.36	9.28	14.43	212.56

935

936

937 Table 6. Molar heat capacities and derived thermodynamic functions of the dehydrated
938 saponite Sap-Ca-1 (corrected for impurities) at selected temperatures.

T	$C°_{p,m}(T)$	$S°(T)$	$H°(T)$-$H°(298.15)$
K	J/(K·mol)	J/(K·mol)	kJ/mol
0	0.00	0.00	-51.608
10	2.14	0.57	-51.603
20	5.42	3.46	-51.560
30	9.74	6.27	-51.489
40	18.23	10.18	-51.351
50	29.04	15.35	-51.117
60	41.69	21.74	-50.764
70	56.05	29.22	-50.277
80	71.49	37.71	-49.640
90	87.60	47.05	-48.845
100	104.10	57.13	-47.887
110	120.58	67.82	-46.764
120	136.92	79.02	-45.476
130	153.02	90.61	-44.026
140	168.58	102.52	-42.418
150	183.76	114.67	-40.656
160	198.40	127.01	-38.745
170	212.43	139.46	-36.690
180	225.84	151.98	-34.498
190	238.81	164.55	-32.173
200	251.26	177.12	-29.722
210	263.26	189.67	-27.149
220	274.62	202.18	-24.460
230	285.28	214.62	-21.660
240	295.36	226.98	-18.757
250	305.32	239.23	-15.756
260	315.52	251.40	-12.653
270	324.01	263.47	-9.453
280	332.64	275.41	-6.171
290	340.97	287.22	-2.803
298.15	347.20	296.76	0.000
300	348.59	298.91	0.644
310	356.09	310.46	4.168
320	363.18	321.88	7.763
330	370.56	333.16	11.430
340	376.65	344.31	15.165
350	382.99	355.32	18.963
360	389.13	366.20	22.826
370	395.39	376.95	26.749
380	400.69	387.56	30.729
390	406.37	398.04	34.765
400	411.79	408.40	38.856
410	416.96	418.63	42.999
420	421.90	428.74	47.194
430	426.63	438.72	51.437
440	431.16	448.58	55.726
450	435.51	458.32	60.059
460	439.69	467.94	64.435

470	443.70	477.44	68.853
480	447.57	486.82	73.309
490	451.30	496.09	77.803
500	454.89	505.24	82.334
510	458.36	514.29	86.901
520	461.71	523.22	91.501

939

940

941 Table 7. Molar heat capacities and derived thermodynamic functions of the dehydrated Santa

942 Olalla vermiculite (corrected for impurities) at selected temperatures.

T	$C°_{p,m}(T)$	$S°(T)$	$H°(T)$-$H°(298.15)$
K	J/(K·mol)	J/(K·mol)	kJ/mol
0	0.00	0.00	-52.062
10	0.91	0.80	-52.057
20	4.12	2.23	-52.035
30	10.18	4.96	-51.966
40	18.71	9.00	-51.823
50	29.81	14.32	-51.583
60	43.09	20.90	-51.220
70	57.95	28.64	-50.715
80	73.83	37.41	-50.057
90	90.34	47.05	-49.237
100	107.03	57.43	-48.250
110	123.69	68.42	-47.096
120	140.12	79.89	-45.777
130	156.20	91.74	-44.295
140	171.73	103.89	-42.655
150	186.81	116.25	-40.862
160	201.24	128.77	-38.922
170	215.16	141.39	-36.839
180	228.45	154.07	-34.621
190	241.14	166.76	-32.272
200	253.31	179.44	-29.799
210	264.85	192.08	-27.208
220	275.86	204.66	-24.504
230	286.41	217.16	-21.692
240	296.57	229.57	-18.776
250	306.17	241.87	-15.762
260	315.62	254.06	-12.653
270	324.27	266.14	-9.454
280	333.02	278.08	-6.170
290	340.63	289.90	-2.801
298.15	346.70	299.42	0.000
300	348.17	301.57	0.643
310	354.87	313.10	4.159
320	362.06	324.48	7.743
330	367.72	335.73	11.396
340	375.31	346.82	15.111
350	382.49	357.80	18.900
360	389.29	368.67	22.760

370	395.76	379.43	26.685
380	401.92	390.07	30.674
390	407.78	400.58	34.723
400	413.38	410.98	38.829
410	418.74	421.25	42.989
420	423.87	431.40	47.203
430	428.78	441.43	51.466
440	433.50	451.35	55.778
450	438.04	461.14	60.135
460	442.40	470.82	64.538
470	446.60	480.38	68.983
480	450.66	489.82	73.469
490	454.57	499.15	77.996
500	458.35	508.37	82.560
510	462.00	517.49	87.162
520	465.54	526.49	91.800

943

944

945 Table 8. Molar heat capacities and derived thermodynamic functions of the dehydrated
946 nontronite Nau-1 (corrected for impurities) at selected temperatures.

T K	$C°_{p,m}(T)$ J/(K·mol)	$S°(T)$ J/(K·mol)	$H°(T)$-$H°(298.15)$ kJ/mol
0	0.00	0.00	-51.522
10	1.67	0.98	-51.516
20	10.38	3.80	-51.470
30	16.39	9.03	-51.339
40	25.47	14.92	-51.132
50	37.82	21.86	-50.819
60	51.60	29.95	-50.373
70	66.30	39.00	-49.784
80	81.65	48.84	-49.046
90	97.20	59.35	-48.152
100	112.79	70.40	-47.102
110	128.18	81.87	-45.897
120	143.20	93.67	-44.540
130	157.69	105.71	-43.035
140	171.76	117.91	-41.387
150	185.35	130.23	-39.601
160	198.37	142.61	-37.683
170	210.92	155.01	-35.635
180	223.06	167.41	-33.465
190	234.60	179.79	-31.176
200	245.77	192.10	-28.774
210	256.48	204.36	-26.262
220	266.79	216.53	-23.645
230	276.81	228.62	-20.926
240	286.34	240.60	-18.110
250	295.50	252.47	-15.201
260	304.20	264.24	-12.202
270	312.65	275.88	-9.117
280	320.75	287.39	-5.950
290	328.56	298.79	-2.703
298.15	335.16	307.98	0.000
300	336.45	310.06	0.621
310	343.85	321.21	4.022
320	351.61	332.25	7.500
330	358.79	343.18	11.053
340	365.48	353.99	14.674
350	371.71	364.68	18.361
360	377.55	375.23	22.107
370	383.05	385.65	25.911
375	385.68	390.81	27.832

947

948

949 Table 9. Enthalpies of dissolution of the clay samples and of the corresponding secondary
950 reference constituents* and impurities mixtures (* = except for H_2O)

		Mass (mg)	ΔH_{diss} (J/g)	Mean ΔH_{diss} (J/g)
Saponite Sap-Ca-1 Experiments in HF(6M) – HNO_3 (7M)	Dehydrated sample	39.65 39.64 40.05 40.22	-2291.09 -2287.32 -2289.98 -2287.55	-2288.99 (± 2.56)
	Mixture of constituents* + impurities	44.56 44.55 44.54 44.54 44.55	-2200.69 -2187.55 -2191.19 -2202.17 -2196.32	-2195.58 (± 7.13)
Nontronite Nau-1 Experiments in HF(6M) – HNO_3 (7M)	Dehydrated sample	39.06 39.56 39.94 40.03 39.78	-1956.37 -1955.54 -1958.15 -1945.54 -1958.75	-1954.87 (± 6.18)
	Mixture of constituents* + impurities	42.24 42.22 42.06 42.19 42.21	-1792.11 -1787.94 -1799.08 -1794.10 -1791.20	-1792.88 (± 4.73)
	Hydrated nontronite n = 5.978	40.33 40.30 40.29 40.38 39.91	-1558.08 -1553.10 -1553.77 -1552.27 -1548.09	-1553.06 (± 4.11)
Santa Olalla vermiculite Experiments in HF(3M) – HNO_3(10M)	Dehydrated sample	40.03 39.49 39.55 39.52 40.38	-2440.80 -2455.19 -2449.72 -2453.70 -2455.94	-2451.07 (± 7.15)
	Mixture of constituents* + impurities	47.36 47.35 47.38 47.36 47.36	-2083.98 -2080.17 -2081.44 -2075.63 -2078.83	-2080.01 (± 3.56)
Note: Uncertainties between brackets are calculated using Student's *t*-distribution with a 95% confidence interval				

951
952
953
954

955 Table 10. Reactions of formation of clay minerals from the secondary reference constituents

956 and associated enthalpies $\Delta H°_{f/constit.}$, in kJ/mol (at 1 bar and 298.15 K).

	Reactions of formation of clay minerals	$\Delta H°_{f/constit.}$ (kJ/mol)
Saponite Sap-Ca-1 (n = 0)	$0.038\ Ca(OH)_2 + 3.372\ SiO_2 + 0.397\ Al(OH)_3 + 2.948\ Mg(OH)_2 + 0.021\ FeO + 0.034\ FeOOH,0.225H_2O + 0.001\ MnO + 0.197\ Na_2SiO_3 + 0.021\ KOH = Ca_{0.038}Na_{0.394}K_{0.021}(Si_{3.569}Al_{0.397}Fe^{3+}_{0.034})(Mg_{2.948}Fe^{2+}_{0.021}Mn_{0.001})O_{10}(OH)_2 + 2.617\ H_2O$	-59.01 (± 3.50)
Nontronite NAu-1 (n = 0)	$0.247\ Ca(OH)_2 + 3.458\ SiO_2 + 0.810\ Al(OH)_3 + 0.066\ Mg(OH)_2 + 1.688\ FeOOH + 0.020\ KNO_3 + 0.007\ TiO_2 = Ca_{0.247}K_{0.020}(Si_{3.458}Al_{0.542})(Al_{0.268}Mg_{0.066}Fe^{3+}_{1.688}Ti_{0.007})O_{10}(OH)_2 + 1.362\ H_2O + 0.020\ HNO_3$	32.44 (± 4.20)
Nontronite NAu-1 (n = 5.978)	$0.247\ Ca(OH)_2 + 3.458\ SiO_2 + 0.810\ Al(OH)_3 + 0.066\ Mg(OH)_2 + 1.688\ FeOOH + 0.020\ KNO_3 + 0.007\ TiO_2 + 4.616\ H_2O = Ca_{0.247}K_{0.020}(Si_{3.458}Al_{0.542})(Al_{0.268}Mg_{0.066}Fe^{3+}_{1.688}Ti_{0.007})O_{10}(OH)_2,5.978H_2O + 0.020\ HNO_3$	-2.28 (± 4.40)
Santa Olalla vermiculite (n = 0)	$2.778\ SiO_2 + 1.414\ Al(OH)_3 + 2.468\ Mg(OH)_2 + 0.226\ FeOOH + 0.028\ FeO + 0.445\ Ca(OH)_2 + 0.018\ TiO_2 + 0.007\ MnO = Ca_{0.445}(Si_{2.778}Al_{1.222})(Al_{0.192}Mg_{2.468}Fe^{3+}_{0.226}Fe^{2+}_{0.028}Ti_{0.018}Mn_{0.007})O_{10}(OH)_2 + 4.147\ H_2O$	10.39 (± 5.50)

Notes: M_{min}(saponite) = 391.148 g/mol; η(saponite) = 0.96635; M_{min}(nontronite) = 419.842 g/mol; η(nontronite) = 0.90370; M_{min}(vermiculite) = 403.465 g/mol; η(vermiculite) = 0.99467; M_{H2O} = 18.02 g/mol; M_{HNO3} = 63.01 g/mol . For overall reactions, the SiO_2 amount is divided into 52.5 mol% of quartz and 47.5 mol% of cristobalite. Standard uncertainties given between brackets correspond to one standard deviation of the means.

957

Table 11. – Thermodynamic properties of the minerals nontronite NAu-1, saponite Sap-Ca-1 and Santa Olalla vermiculite, at different hydration states, at 1 bar and 298.15 K. For the given temperature ranges, the $Cp(T)$ functions of the clay minerals are expressed according to $C_p(T) = A + 10^{-3}\ B\ T + 10^{5}\ C\ T^{-2}$, where A, B and C are Maier-Kelley coefficients, obtained by fitting the Cp curves of the minerals.

Mineral	ΔG_f^0 kJ/mol	ΔH_f^0 kJ/mol	$S^{0(cal)}$ J/(K·mol)	$S^{0(conf)}$ J/(K·mol)	S^0 J/(K·mol)	$C_p{}^0$(298.15K) J/(K·mol)	A J/(K·mol)	B J/(K^2·mol)	C (J.K)/mol	*T range for Cp functions*
Nontronite NAu-1 $n^*=0$	-4683.56 (± 5.73)	-5034.39 (± 5.33)	307.98 (± 7.04)	24.87	332.85 (± 7.04)	335.16 (± 0.33)	289.81	363.02	-55.91	298 – 375 K
Nontronite NAu-1 $n^*=5.978$		-6774.32 (±5.61)								
Saponite Sap-Ca-1 $n^*=0$	-5622.24 (± 4.88)	-5993.84 (± 4.86)	296.76 (± 1.56)	17.83	314.59 (± 1.56)	347.20 (± 1.74)	347.26	274.68	-73.05	298 – 520 K
Santa Olalla vermiculite $n^*=0$	-5662.23 (± 5.71)	-6030.34 (±5.70)	299.42 (± 0.48)	26.66	326.08 (± 0.48)	346.70 (± 0.35)	329.29	313.22	-67.82	298 – 520 K
Properties recalculated for simplified structural formulae†										
Nontronite NAu-1 $n^*=0$	-4684.80 (± 5.74)	-5035.69 (± 5.34)	307.88 (± 7.04)	24.87	332.75 (± 7.04)	335.17 (± 0.34)	289.85	363.09	-55.96	298 – 375 K
Saponite Sap-Ca-1 $n^*=0$	-5622.44 (± 4.88)	-5994.06 (± 4.86)	296.72 (± 1.56)	17.83	314.55 (± 1.56)	347.19 (± 1.74)	347.26	274.68	-73.06	298 – 520 K
Santa Olalla vermiculite $n^*=0$	-5666.17 (± 5.74)	-6034.41 (±5.73)	299.11 (± 0.48)	26.66	325.77 (± 0.48)	346.73 (± 0.35)	329.42	313.40	-67.98	298 – 520 K

Notes: * n is the number of moles of water per mole of clay (on the basis $O_{10}(OH)_2$)

† Simplified formulae are introduced in order to ease the predictive calculations and their implementation into databases. The simplification process is detailed further in the text

Standard uncertainties associated with ΔH_f^0 and ΔG_f^0 correspond to one standard deviation of the means, calculated according to the error propagation method described in Ellison et al. (2000).

963 **FIGURES**
964

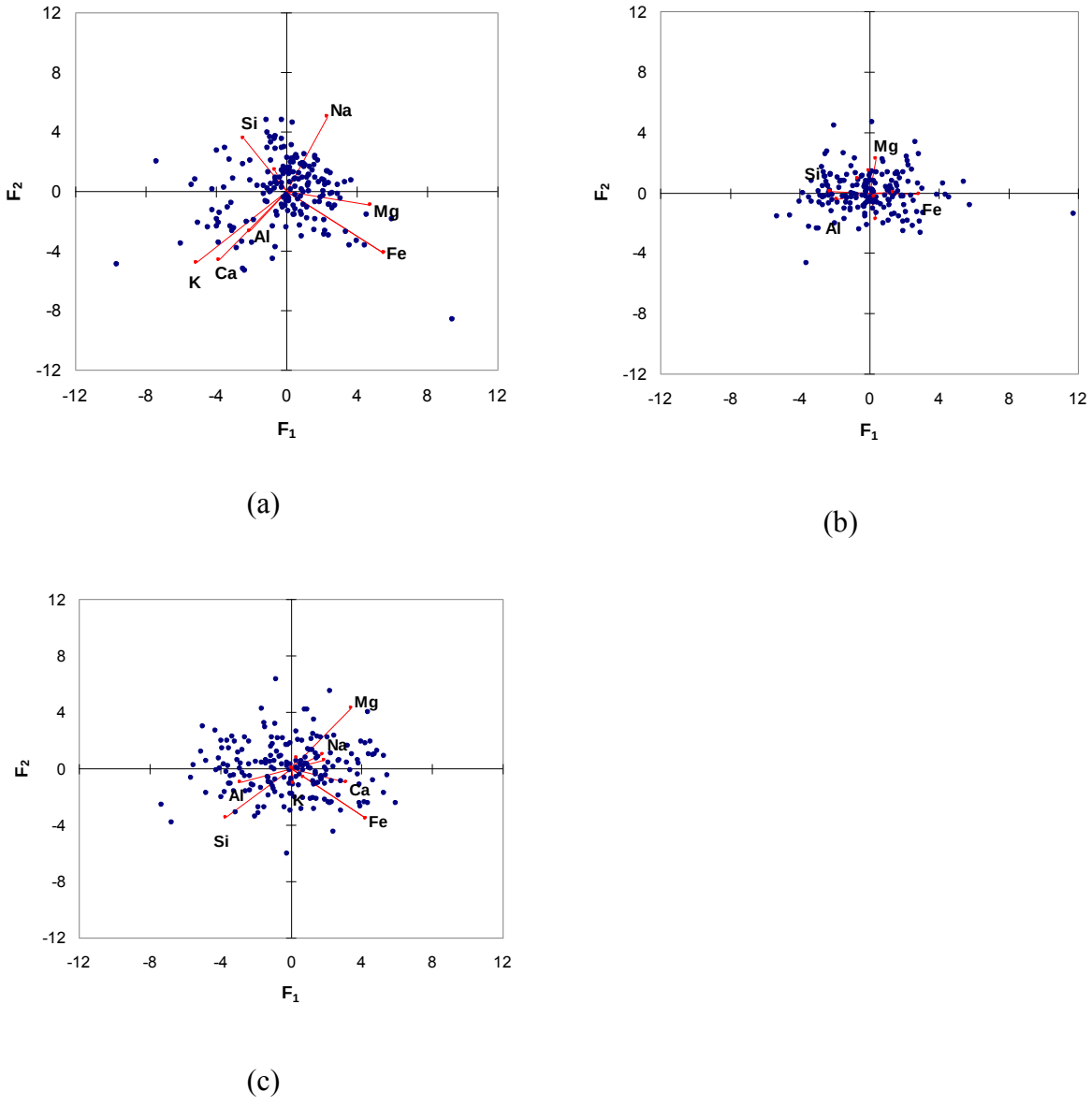

965 Figure 1. Statistical treatment by the PCA method of the microprobe analyses of (a)
966 saponite Sap-Ca-1, (b) nontronite NAu-1 and (c) Santa Olalla vermiculite. Biplot
967 representations of individuals and variables onto plans defined by the eigenvectors ($\mathbf{F_1}$, $\mathbf{F_2}$).

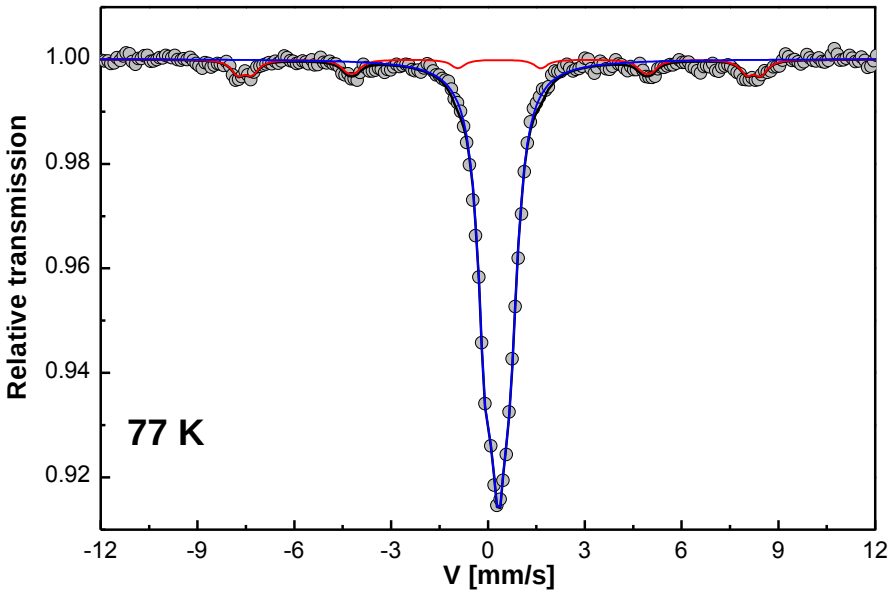

968

969 Figure 2. ^{57}Fe Mössbauer spectrum at 77 K for the nontronite NAu-1 sample (in red,

970 magnetic component for Fe^{3+} in goethite; in blue, component for Fe^{3+} in nontronite).

971

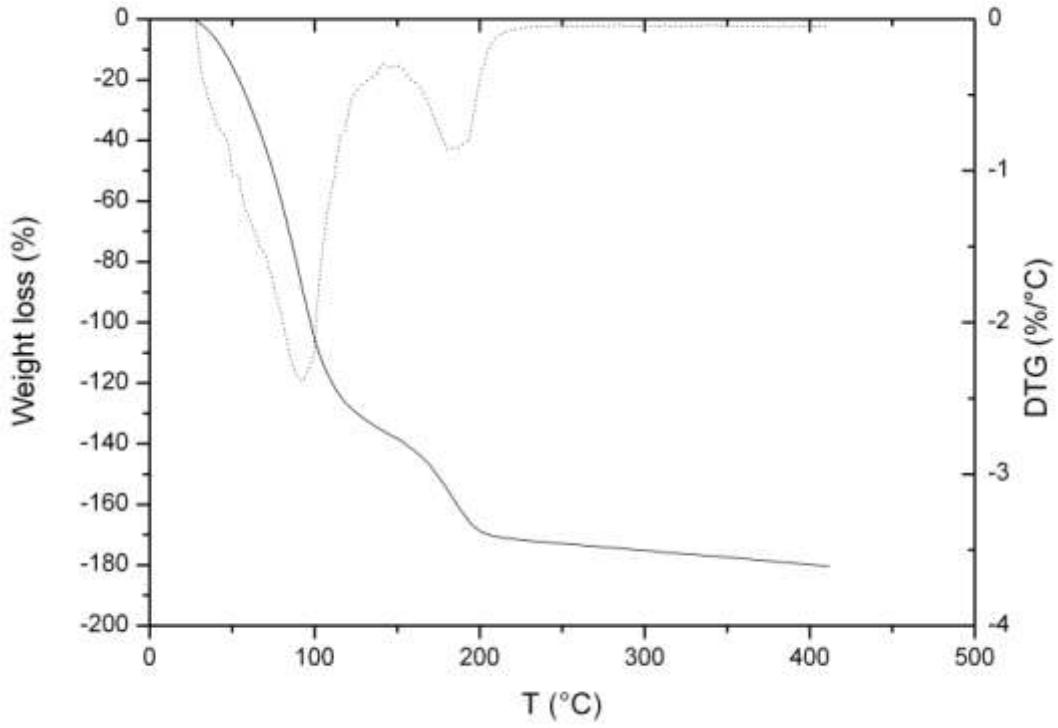

Figure 3. TGA curves for the powdered Ca-vermiculite from Santa Olalla. Temperature dependence of the weight loss (solid line) and the derivative of weight loss versus temperature (dashed line) showing two peaks at 90 °C and 185 °C.

977

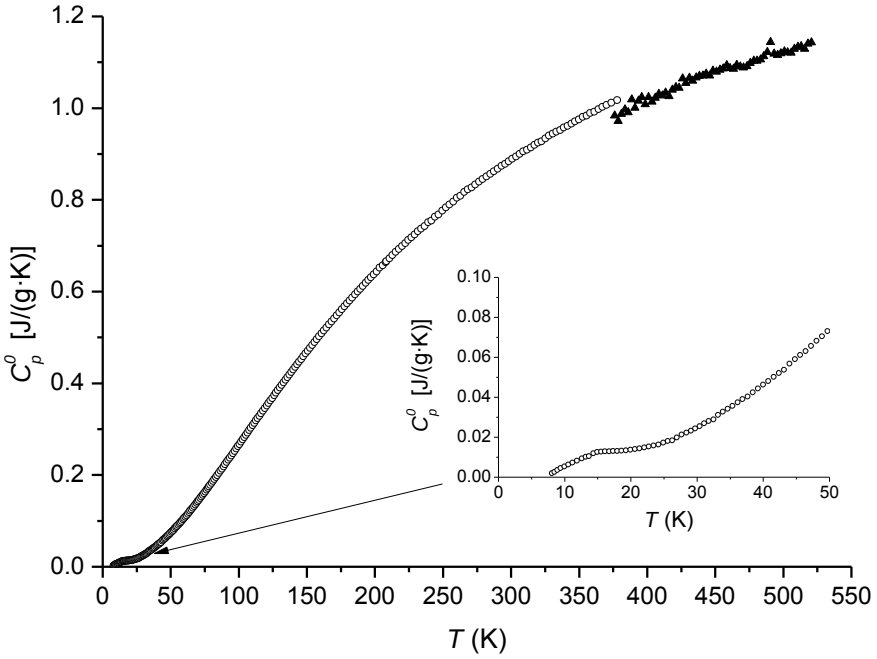

(a)

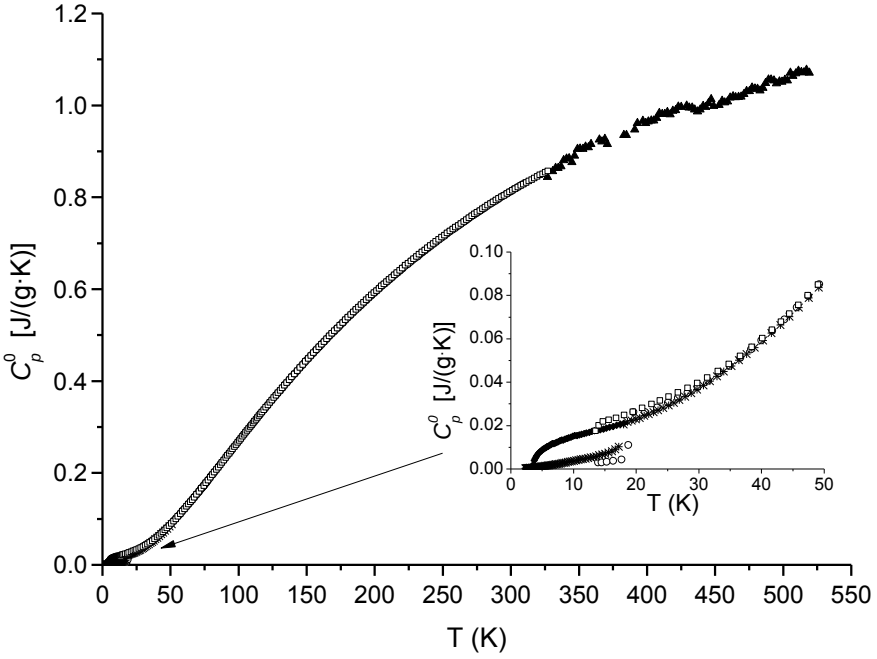

(b)

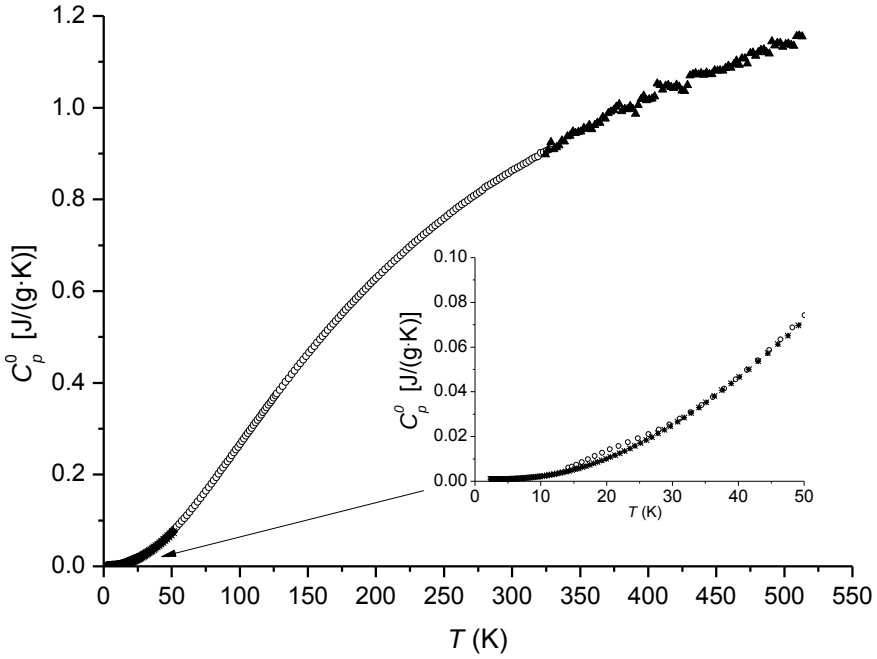

(c)

978 Figure 4. Measured heat capacities of samples (including impurities) (a) saponite Sap-
979 Ca-1; (b) nontronite NAu-1; (c) Santa Olalla vermiculite. (Circles: low-TAC; up triangles:
980 DSC; crosses: PPMS by heating; black diamonds: PPMS by cooling).
981

982

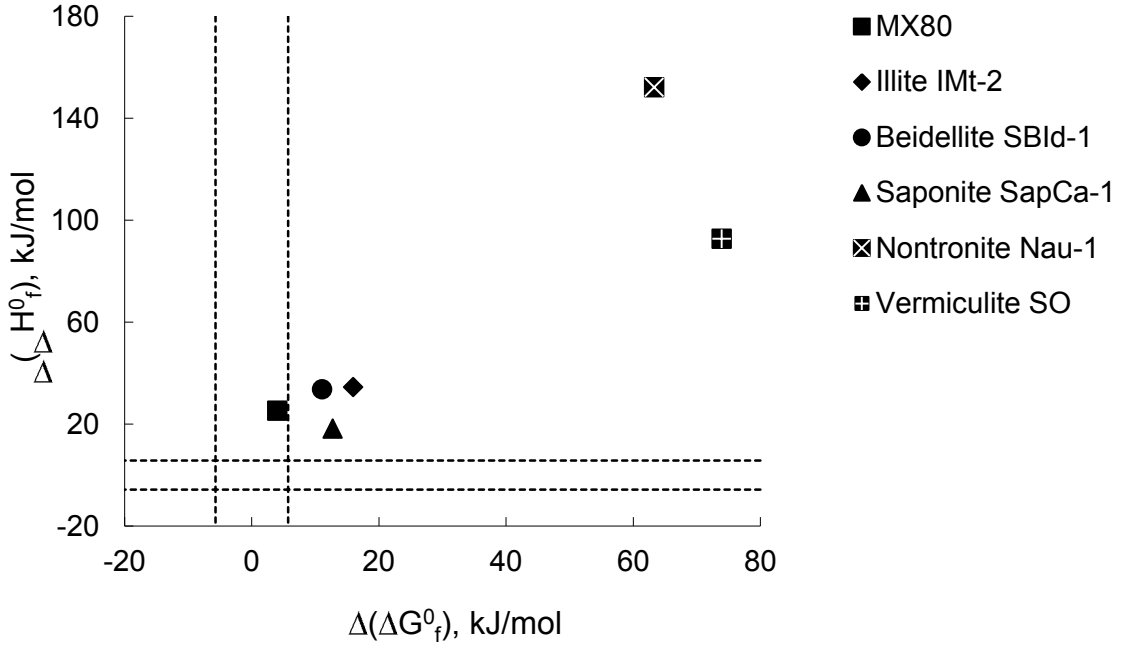

983

984 Figure 5. Discrepancy between experimental and predicted values of the Gibbs free
985 energy $\Delta(\Delta G^0_f)$ and the enthalpy of formation $\Delta(\Delta H^0_f)$ of 6 clay minerals, at 298.15 K and 1
986 bar. Experimental measurements are from Gailhanou et al. (2012) for the smectite MX80, the
987 illite IMt-2 and the beidellite SBId-1. For the nontronite NAu-1, the Santa Olalla vermiculite
988 (vermiculite SO) and the saponite SapCa-1, the experimental values are obtained in this work.
989 The estimate of ΔG^0_f and ΔH^0_f are calculated using the Chermak and Rimstidt (1989) method.
990 The dotted lines represent an uncertainty interval that could correspond to 1 unit on the 25°C
991 Log*K* equilibrium constant.

992

993

994

995

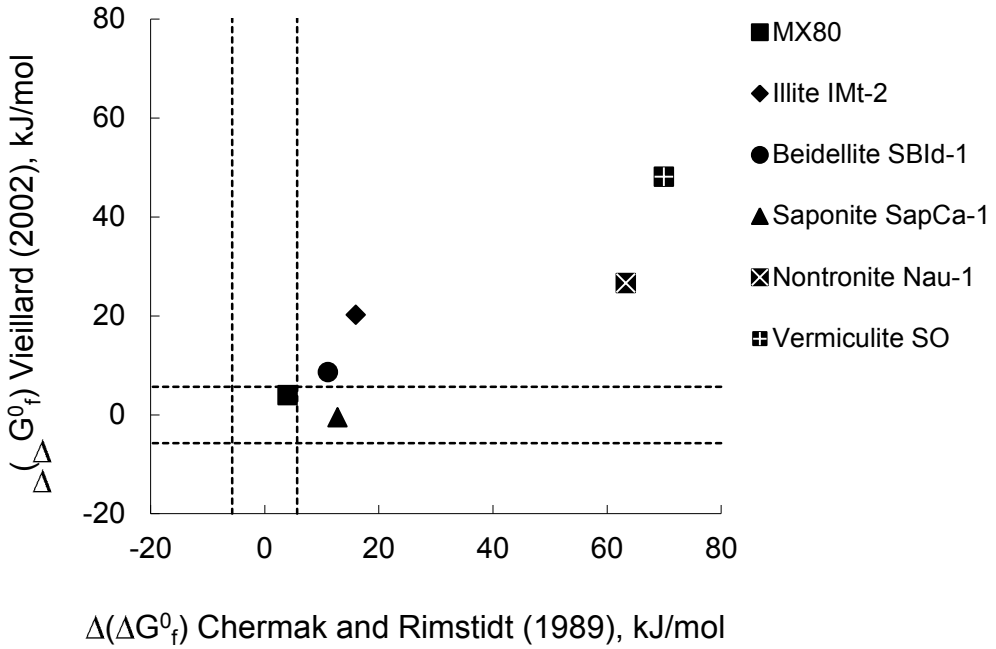

996

997 Figure 6. Discrepancy between experimental and predicted values of the Gibbs free
998 energy $\Delta(\Delta G^0_f)$ for 6 clay minerals, at 298.15 K and 1 bar. Experimental values have the same
999 origin as in Figure 5. The estimates of ΔG^0_f are calculated using the Vieillard (2002) and the
1000 Chermak and Rimstidt (1989) methods. The dotted lines are defined in the same way as in
1001 Figure 5.

1002

1003

1004

1005

1006

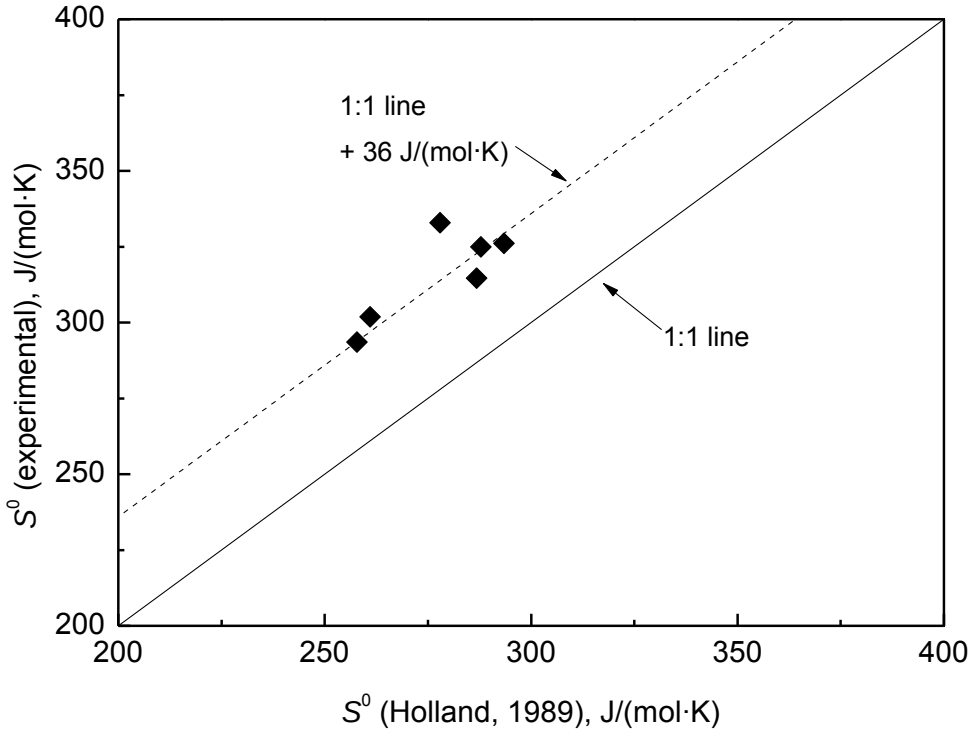

1007

1008 Figure 7. Comparison between experimental and predicted values of the standard
1009 entropy of 6 clay minerals, hydrated and dehydrated, at 298.15 K and 1 bar. Experimental
1010 measurements are from Gailhanou et al. (2007, 2012) for smectite MX80, illite IMt-2 and
1011 beidellite SBId-1. For nontronite NAu-1, Santa Olalla vermiculite and saponite SapCa-1, the
1012 experimental values are obtained in this work. The estimates of S^0 are calculated using the
1013 Holland (1989) method.

1014

1015

1016

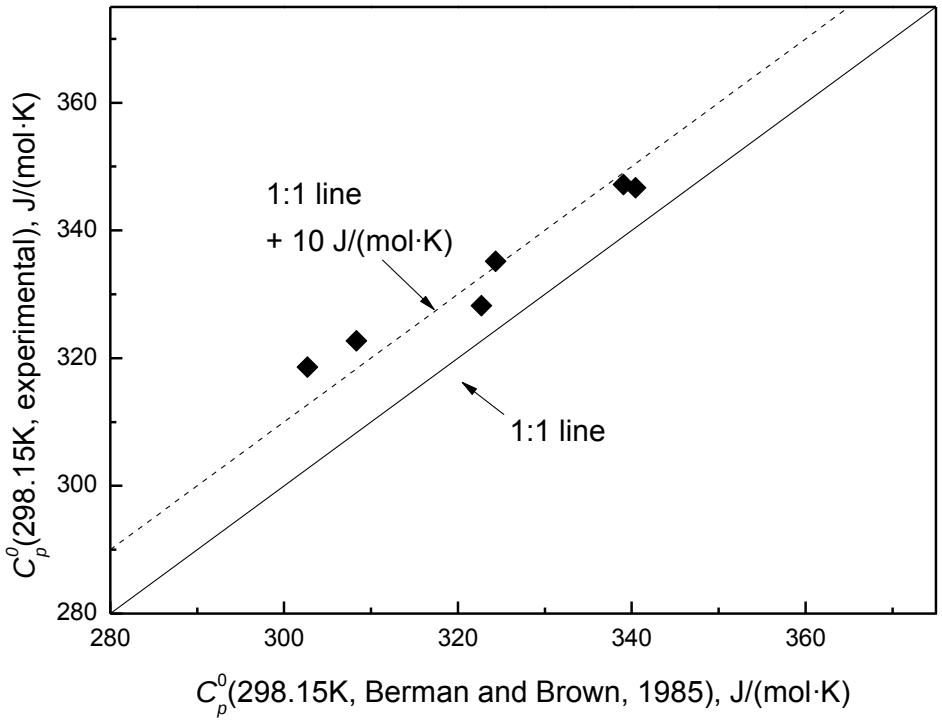

1017

1018 Figure 8. Comparison between experimental and predicted values of the C_p^0(298.15 K)
1019 of 6 clay minerals, hydrated and dehydrated. Experimental measurements have the same
1020 origin as in Figure 9. The estimates of C_p^0(298.15 K) are calculated using the Berman and
1021 Brown (1985) method.

1022

1023

1024

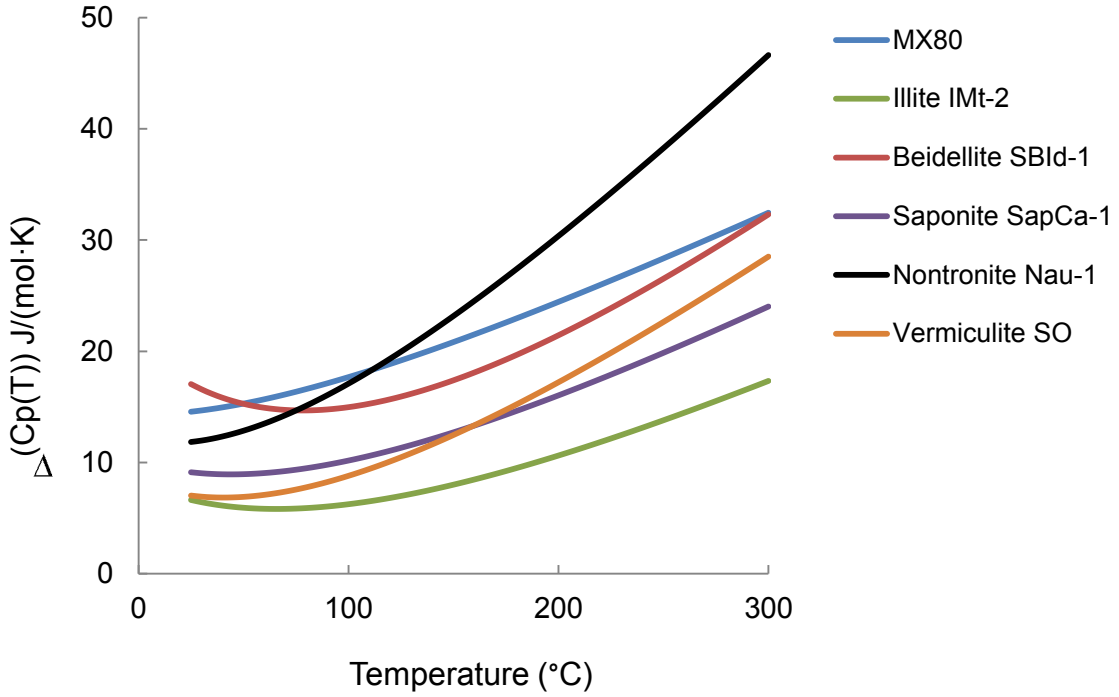

Figure 9. Discrepancy ($\Delta C_p(T)$) between experimental and predicted values of the $C_p^0(T)$ function for 6 clay minerals. Experimental measurements have the same origin as in Figure 9. The estimate of the $C_p^0(T)$ function are calculated using the Berman and Brown (1985) method.